Interpretation of the Microstructure of Steels

H. K. D. H. Bhadeshia

The purpose here is to help identify the microstructures in steel using simple techniques based on the atomic mechanisms by which phases grow from austenite. Apart from their aesthetic beauty, microstructures become meaningful when examined in the context of their metallurgical theory.

The symbols used to represent each phase are as follows:

Phase	Symbol
Austenite	γ
Allotriomorphic ferrite	α
Idiomorphic ferrite	α_I
Pearlite	*P*
Widmanstätten ferrite	α_w
Upper bainite	α_b
Lower bainite	α_{lb}
Acicular ferrite	α_a
Martensite	α'
Cementite	θ

Phase Diagram

We shall interpret microstructrures in the context of the iron-carbon equilibrium phase diagram, even though steels inevitably contain other solutes, whether by design or as impurities. The diagram is nevertheless useful since the transformation behaviour of austenite does not change dramatically unless the steel has a large concentration of solutes.

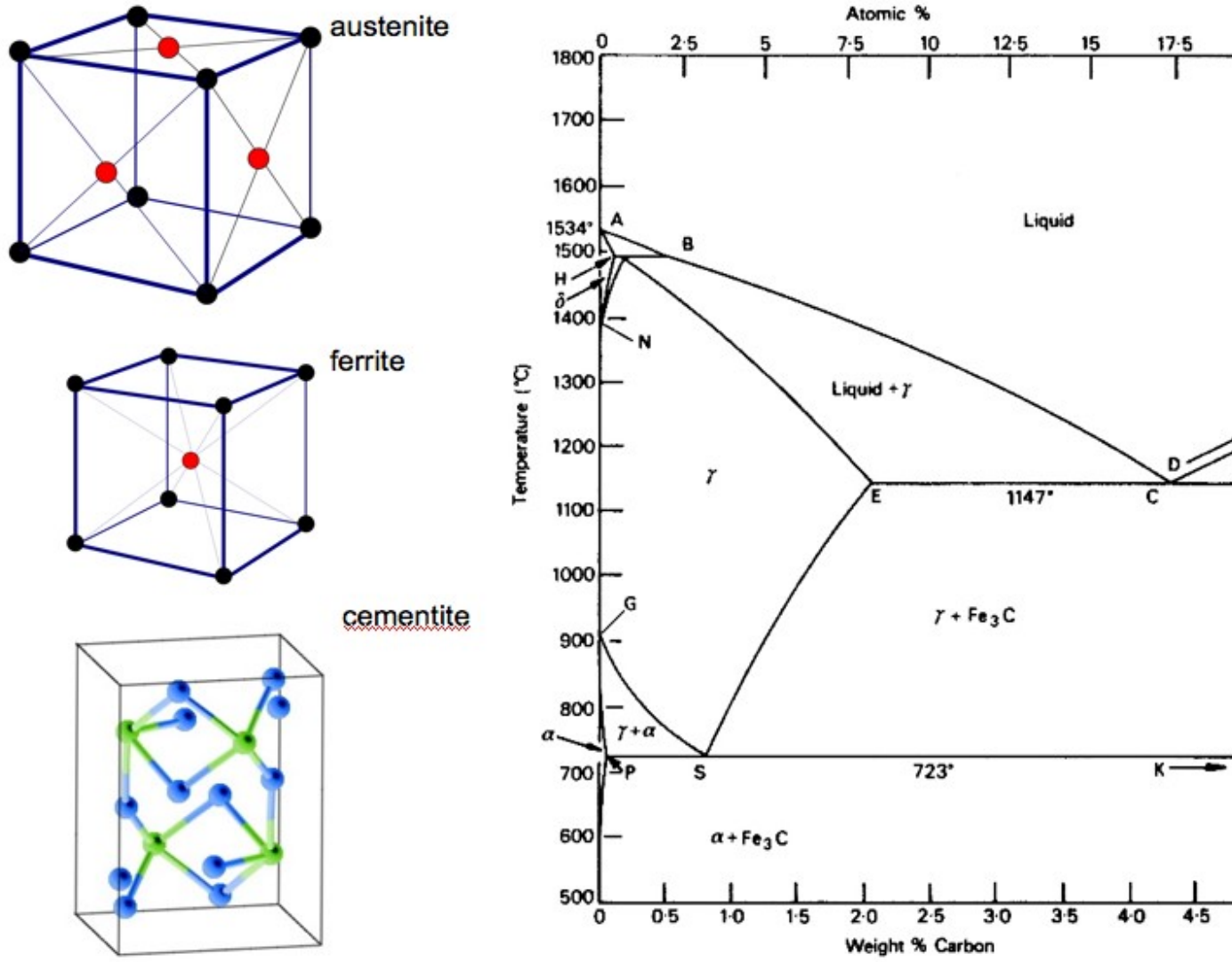

Figure 1: Crystal structures of austenite, ferrite and cementite, and the Fe-C equilibrium phase diagram. Only the front-facing face-centering atoms are illustrated for austenite for the sake of clarity.

Austenite has a cubic-close packed crystal structure, also referred to as a face-centred cubic structure with an atom at each corner and in the centre of each face of the unit cell. Ferrite has a body-centred cubic crystal structure and cementite has an orthorhombic unit cell containing four formula units of Fe_3C. The phase diagram illustrates the domains in which particular phases or combinations of phases are stable, and contains information about their equilibrium compositions. Equilibrium phase fractions can also be estimated from a knowledge of the carbon concentration of the steel and an application of the lever rule.

Steels with a carbon concentration less that the eutectoid marked *S* on the phase diagrm are known as *hypoeutectoid* and those which exceed this concentration are said to be *hypereutectoid*.

Atomic Mechanisms of Transformation

An understanding of the atomic mechanisms of solid-state transformation is important because the details of the way in which atoms move determine the morphology, chemical composition and other characteristics of the microstructure.

Imagine, as illustrated in Fig. 2, that the austenite consists of a mixture of square atoms and round atoms, and has the unit cell outlined in red. One way of changing the crystal structure is to do so without disrupting the relative order of the atoms. This can be done by generating the unit cell of ferrite by a homogeneous deformation of the parent γ. In this *displacive* mechanism, the overall shape of the sample must change in a manner consistent with the change in crystal structure. When this shape deformation occurs in the bulk of a polycrystalline steel, its accommodation leads to a lot of strain energy. This energy can be minimised if the ferrite adopts a thin-plate shape. Since transformation occurs by a deformation, the atoms maintain the sequence which existed in the parent phase. There is therefore, no change in the chemical composition during transformation. There is also a one-to-one atomic correspondence between the ferrite and austenite, which is the basis of the shape memory effect.

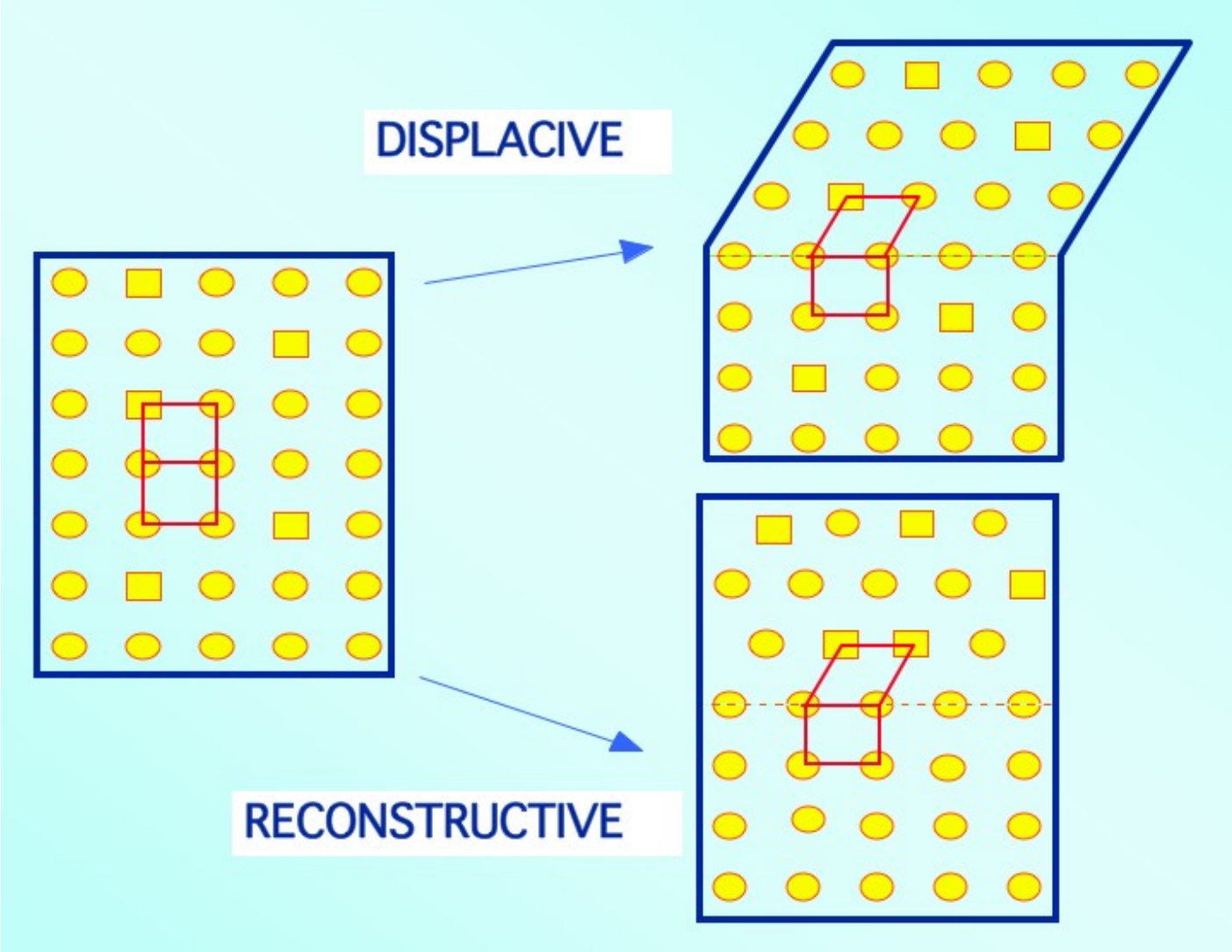

Figure 2: The displacive and reconstructive mechanisms.

The change in crystal structure can also be achieved in effect by breaking the bonds in the austenite and rearranging the atoms into the structure of ferrite whilst maintaining the overall shape. This requires atoms to diffuse over distances comparable to the size of the transformation product. Thus, although the strain energy associated with displacive transformations is avoided, this *reconstructive* mechanism can only occur at temperatures where atoms are sufficiently mobile. Given that atoms are mobile, certain species which are more soluble in a particular phase (α or γ) will tend to migrate preferentially into that phase, leading to a difference in the chemical composition between α and γ. The atomic correspondence between the parent and product phases is lost in a reconstructive transformation. The shape of the transformation product is

either determined by growth circumstances, or as equilibrium is approached, by a minimisation of the overall interfacial energy per unit volume.

Figure 3 illustrates how the major transformation products can be classified according to the atomic mechanisms of transformation. The details of this and the relevance to the interpretation of microstructure will become apparent as this tutorial progresses. One example is that all the displacive transformation products necessairly have a plate shape.

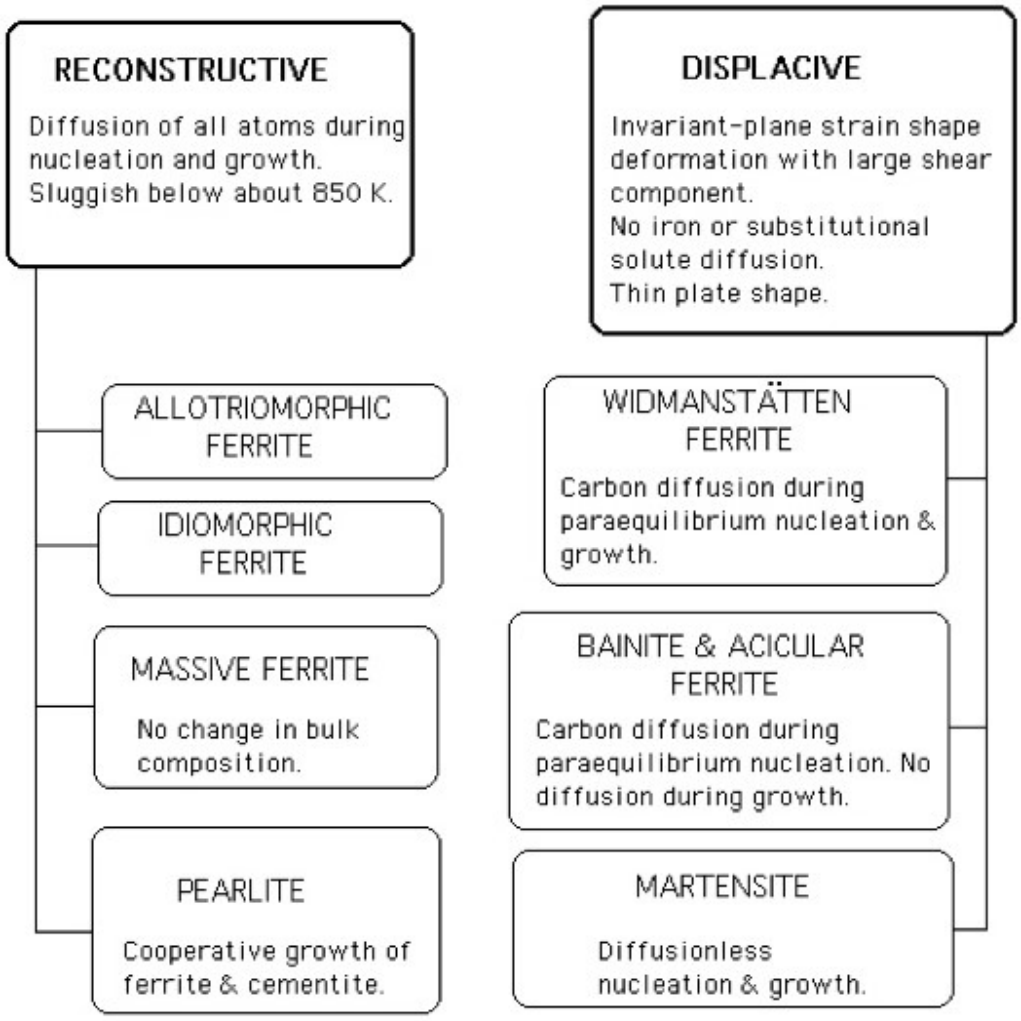

Figure 3: The displacive and reconstructive mechanisms.

Time-Temperature-Transformation Diagram

It is obvious that the equilibrium phase digram (Fig. 1) does not contain any information about phases such as bainite, martensite *etc.* This is because it represents equilibrium whereas the variety of transformation products have a range of deviations from the equilibrium state.

The phase diagram for obvious reasons does not feature time. The kinetics of transformation are better illustrated using a time-temperature-transformation (TTT) diagram as illustrated in Fig. 4. There are two "C" curves, the top one for reconstructive transformations and the lower one for displacive transformations. Also illustrated are schematic microstructures within individual austenite grains.

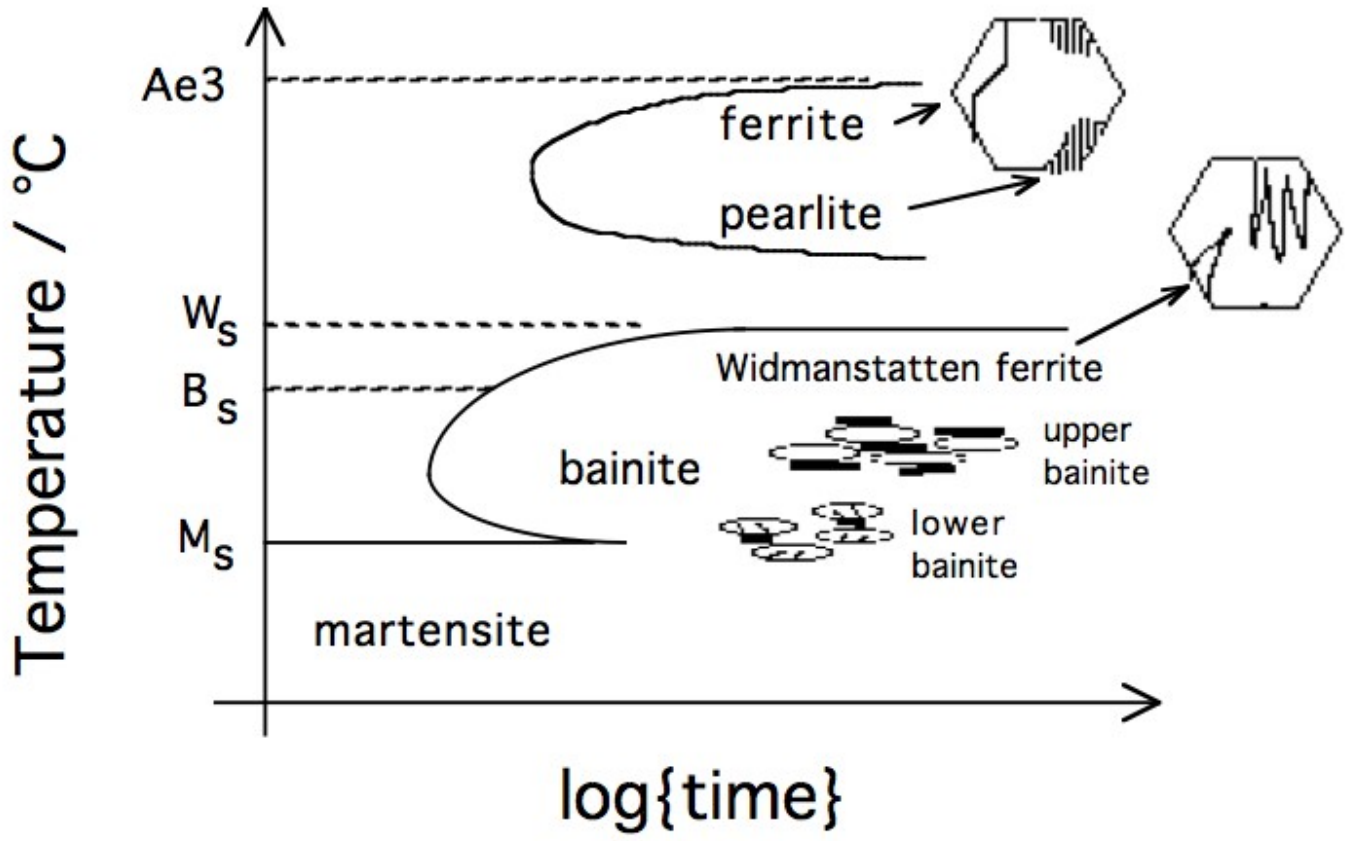

Figure 4: Time-temperature-transformation diagram.

Allotriomorphic and Idiomorphic Ferrite

These are both the products of the reconstructive transformation of austenite, but an allotriomorph forms at an austenite grain surface whereas an idiomorph nucleates somewhere within the grain, out of contact with the grain surface.

The word *allotriomorph* implies that the shape of the ferrite does not reflect its internal crystalline symmetry. This is because it tends to grow more rapidly along the austenite grain surface and hence its contours refect those of the γ grain boundary. In contrast, an *idiomorph* is not influenced by the boundary and hence has a crystallographically facetted shape. This is illustrated schematically in Fig. 5 and actual micrographs of an allotriomorph and idiomorph are presented in Figs. 6, 7.

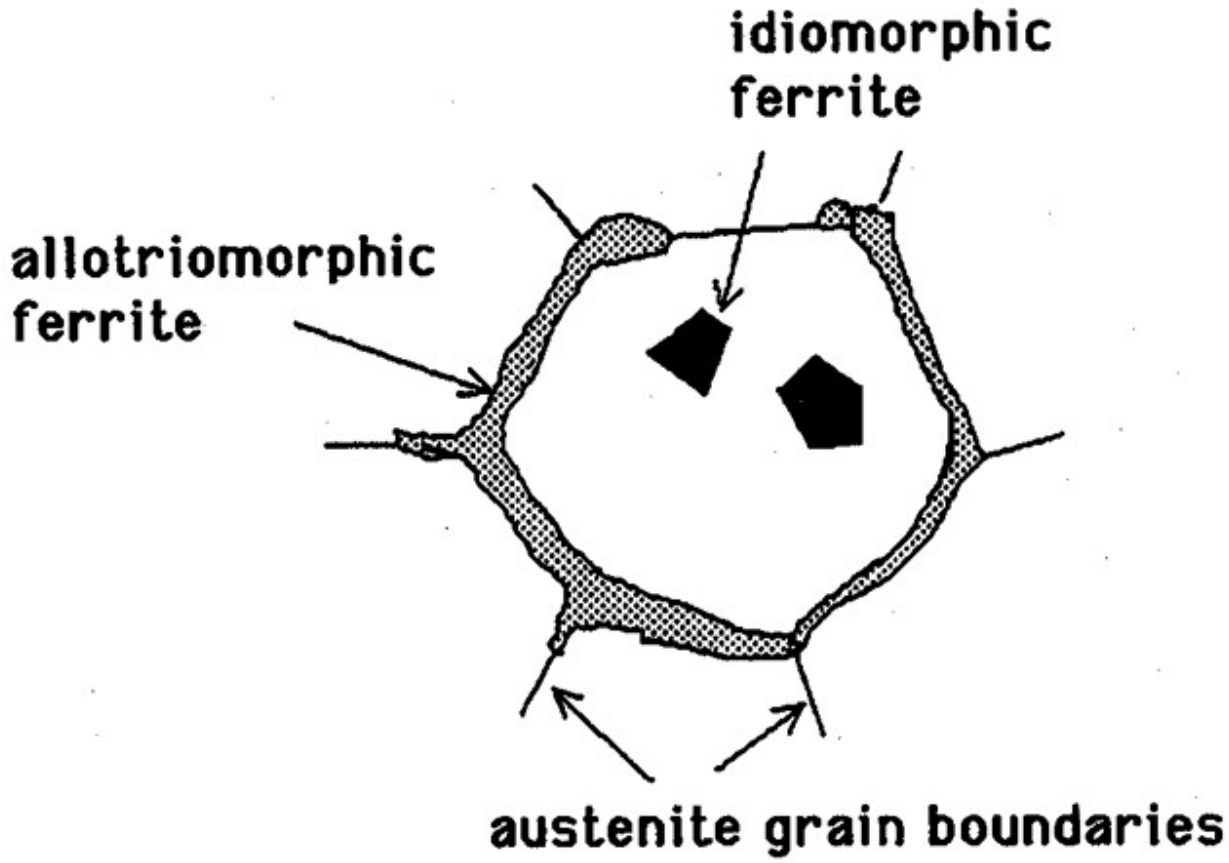

Figure 5: Grain boundary allotriomoph of ferrite, and intragranular idiomorph.

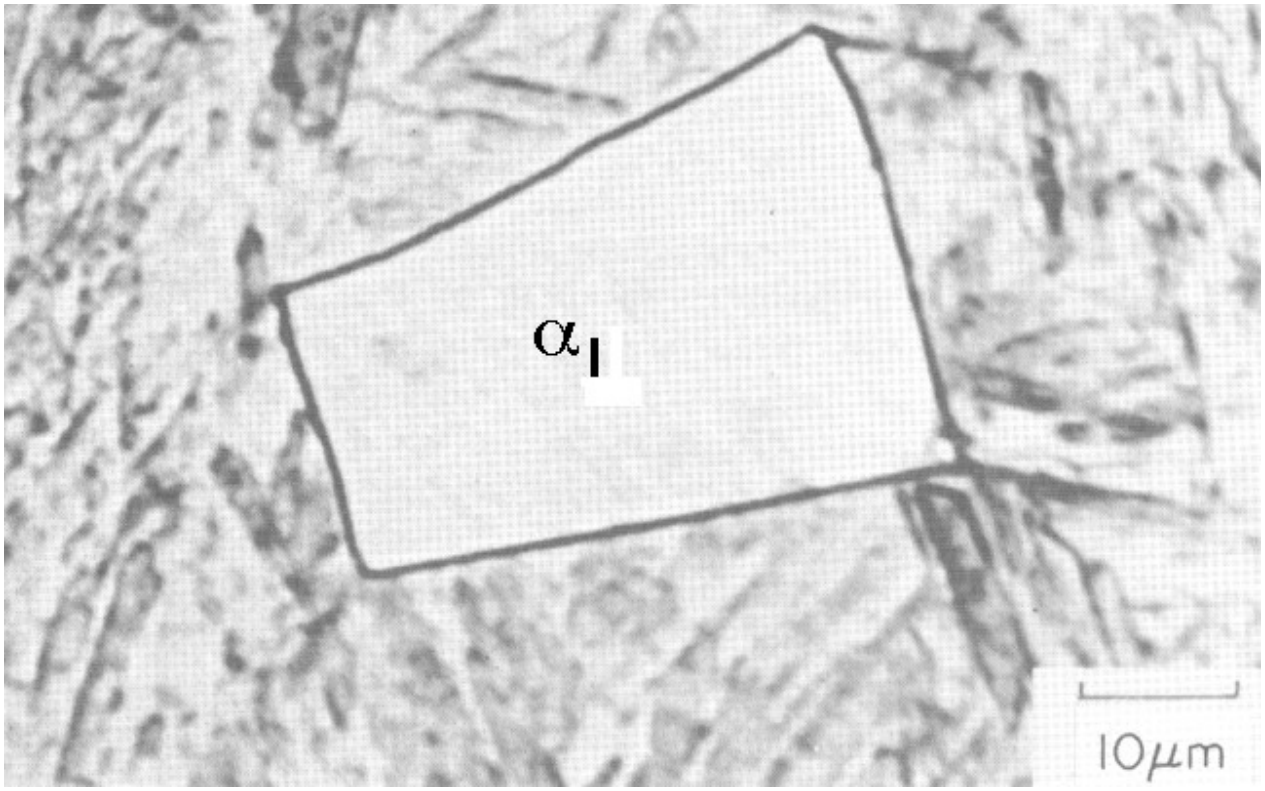

Figure 6: An idiomorph of ferrite in a sample which is partially transformed into α and then quenched so that the remaining γ undergoes martensitic transformation. The idiomorph is crystallographically facetted.

One characteristic of a reconstructive transformation is that the transformation product is not limited to the grain in which it nucleates. The ferrite (or pearlite) can grow across austenite grain boundaries. Thus, the allotriomorph shown in Fig. 7 thickens into both of the adjacent austenite grains. In contrast, displacive transformation products are confined to the grains in which they nucleate. This is because the discipline movement of atoms during transformation cannot be sustained across the austenite grain surfaces.

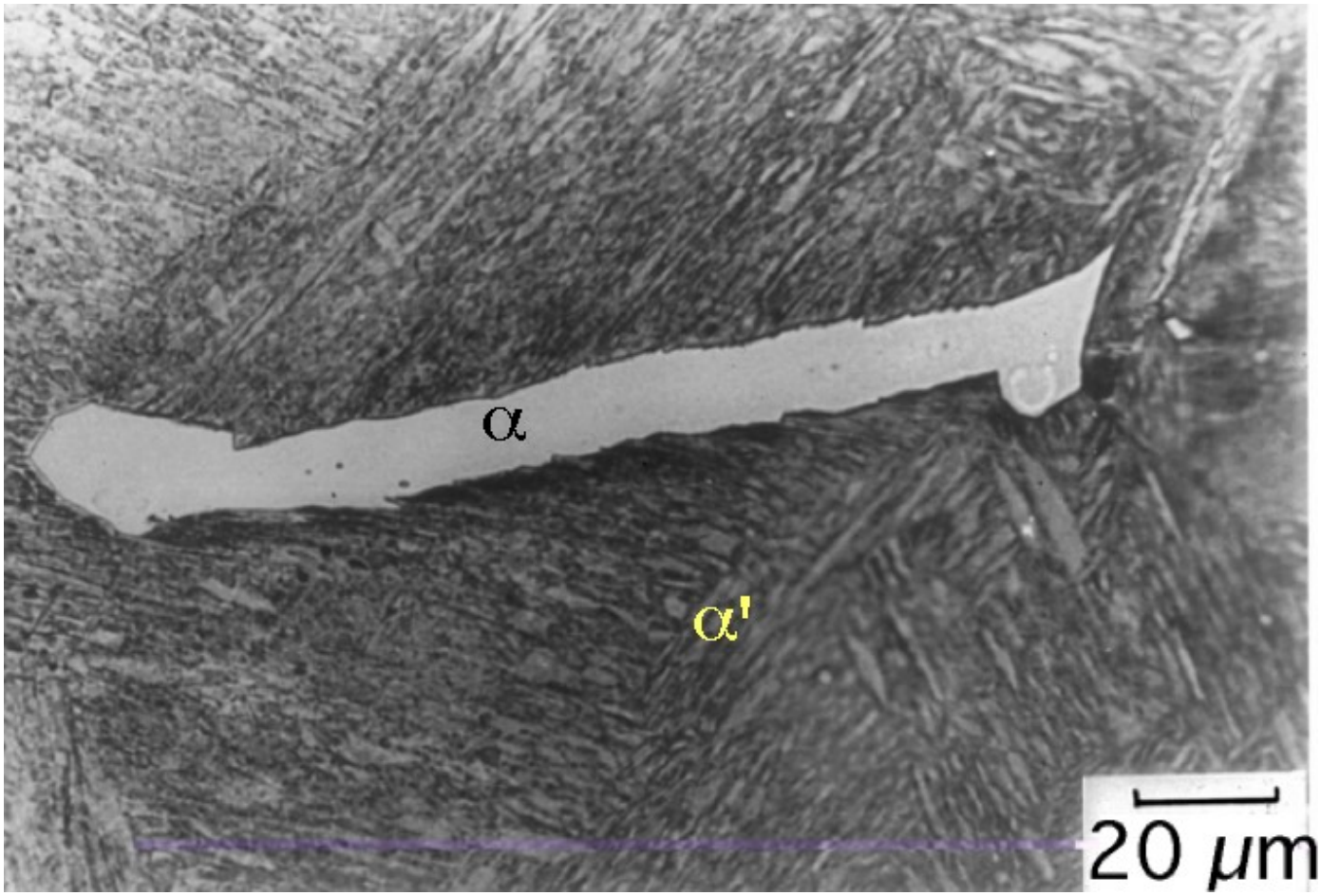

Figure 7: An allotriomorph of ferrite in a sample which is partially transformed into α and then quenched so that the remaining γ undergoes martensitic transformation. The allotriomorph grows rapidly along the austenite grain boundary (which is an easy diffusion path) but thickens more slowly.

As the extent of transformation increases, the shape of the ferrite will change as grains growing from different origins touch each other (impinge). In Fig. 8, the austenite grain boundaries are completely decorated by ferrite allotriomorphs and the residual austenite has transformed into pearlite (which exhibits typical irridescence).

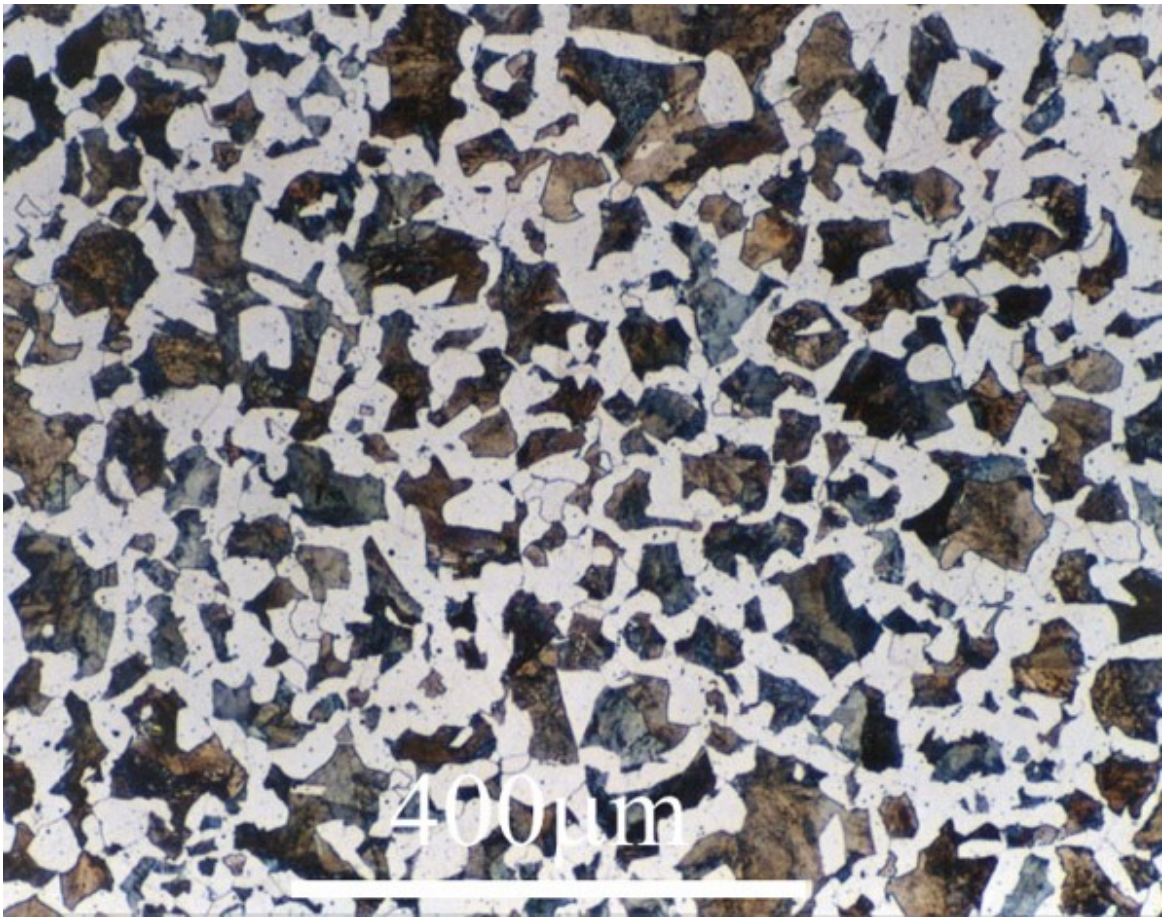

Figure 8: Allotriomorphic ferrite in a Fe-0.4C steel which is slowly cooled; the remaining dark-etching microstructure is fine pearlite. Note that although some α-particles might be identified as idiomorphs, they could represent sections of allotriomorphs. Micrograph courtesy of the DoItPoms project.

In Fig. 9, the low carbon concentration of the steel allows much more allotriomorphic ferrite to form with the grains therefore appearing equiaxed because of the effects of hard impingment. The amount of pearlite is reduced because of the lower carbon concentration of the steel.

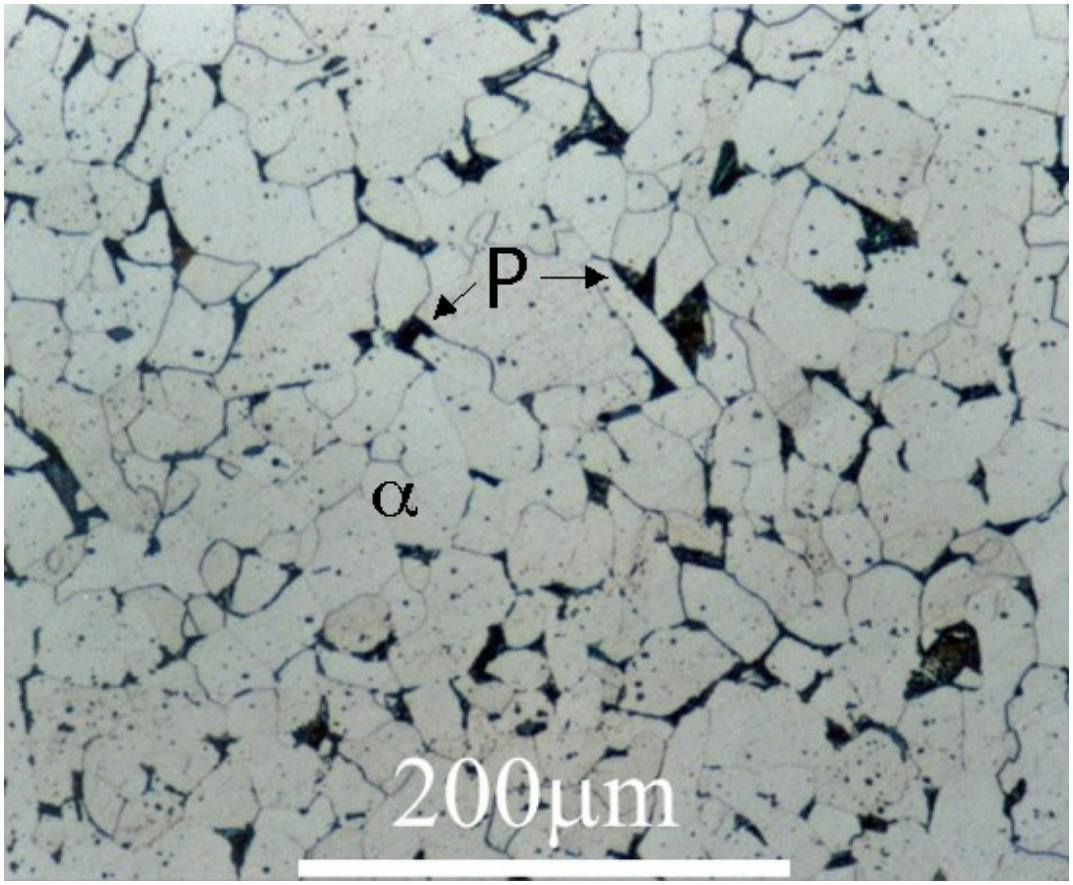

Figure 9: The allotriomorphs have in this slowly cooled low-carbon steel have consumed most of the austenite before the remainder transforms into a small amount of pearlite. Micrograph courtesy of the DoItPoms project. The shape of the ferrite is now determined by the impingement of particles which grow from different nucleation sites.

Pearlite

Pearlite is in fact a mixture of two phases, ferrite and cementite (Fe_3C. It forms by the cooperative growth of both of these phases at a single front with the parent austenite. In Fe-C systems, the average chemical composition of the pearlite is identical to that of the austenite; the latter can therefore completely transform into pearlite.

In a hypoeutectoid steel, a colony of pearlite evolves with the nucleation of ferrite as illustrated in Fig. 10. This in turn triggers the nucleation of a particle of cementite and this process repeats periodically. The two phases then are able to establish cooperative growth at the common front with the austenite, with much of the solute diffusion

happenning parallel to this front within the austenite. The distance between the "layers" of cementite and ferrite is known as the *interlamellar* spacing.

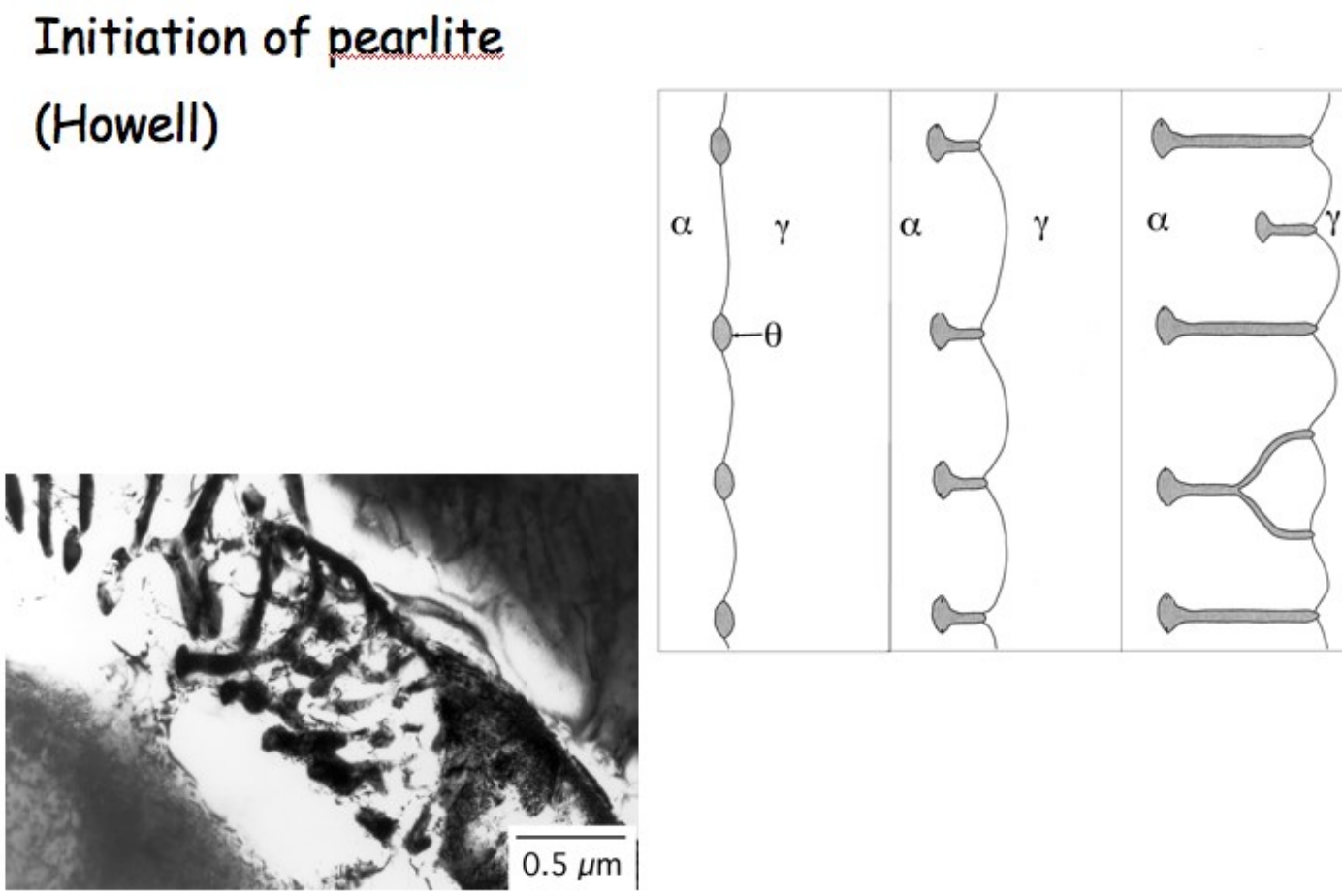

Figure 10: The process by which a colony of pearlite evolves in a hypoeutectoid steel.

The final optical microstructure appears as in Fig. 11, consisting of colonies of pearlite, i.e., regions which participated in cooperative growth at a common front. In this two-dimensional section, each colony appears as if it is a stack of layers of cementite and ferrite. The colonies appear to have different interlamellar spacing, but this may be a sectioning effect.

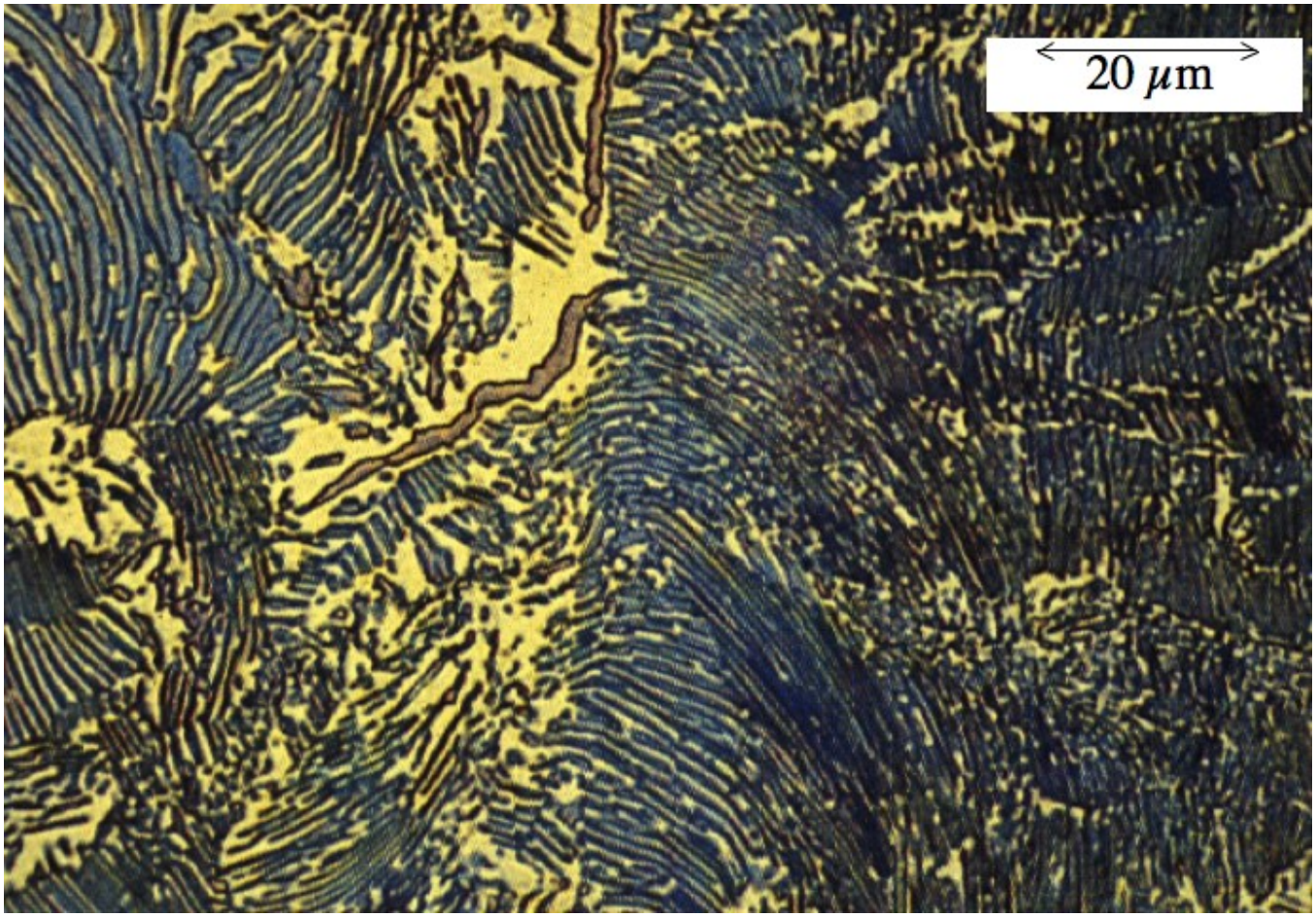

Figure 11: The appearance of a pearlitic microstructure.

Indeed, a colony in three dimensions does not consist of alternating, isolated layers of cementite and ferrite. All of the cementite is a single-crystal, as is all of the ferrite. The colony is therefore an interpenetrating bi-crystal of ferrite and cementite. Imagine in Fig. 12, that the cabbage represents in three dimensions, a single crytal of cementite within an individual colony of pearlite. The leaves of the cabbage are all connected in three dimensions. When the cabbage is immersed in a bucket of water, imagine further that the water is a single crystal of ferrite within the same colony of pearlite. The two will interpenetrate to form the bi-crystal. When this bi-crystal is sectioned, the appearance is that of alternating layers of the two crystals.

.

Figure 12: A cabbage and water analogy of the three-dimensional structure of a single colony of pearlite.

It is important to realise that a colony of pearlite is a bicrystal. Although a steel becomes stronger as the interlamellar spacing is reduced, it does not become tougher because the colony size is what represents the *crystallographic grain size*. Thus, a propagating cleavage crack can pass undeviated across a colony of pearlite.

Figures 13 and 14 show an optical micrograph and a crystallographic orientation image from the same sample. It is evident from the colour image that the colour (crystallographic orientation) is essentially homogeneous within a colony of pearlite.

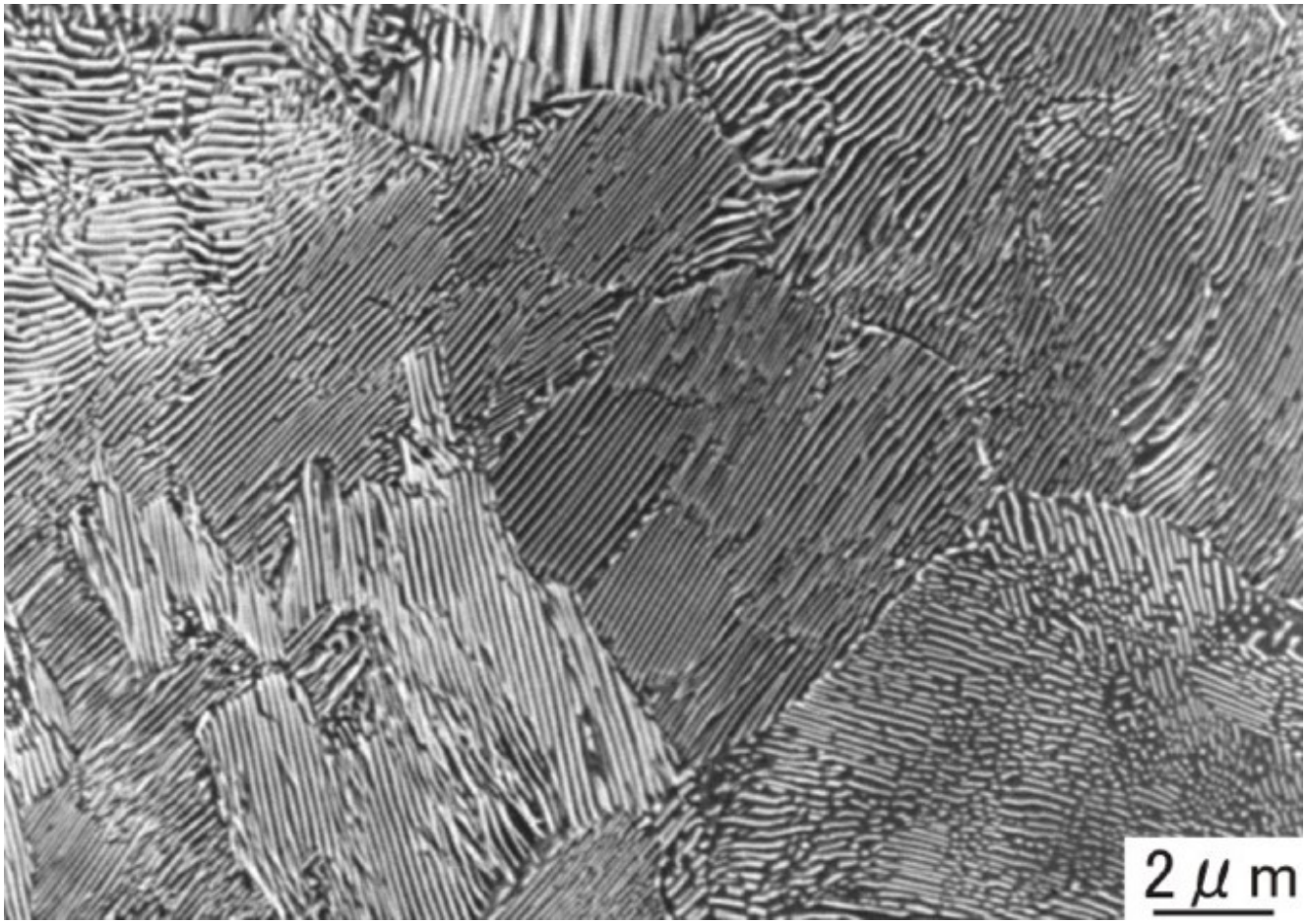

Figure 13: Another optical micrograph showing colonies of pearlite (courtesy S. S. Babu).

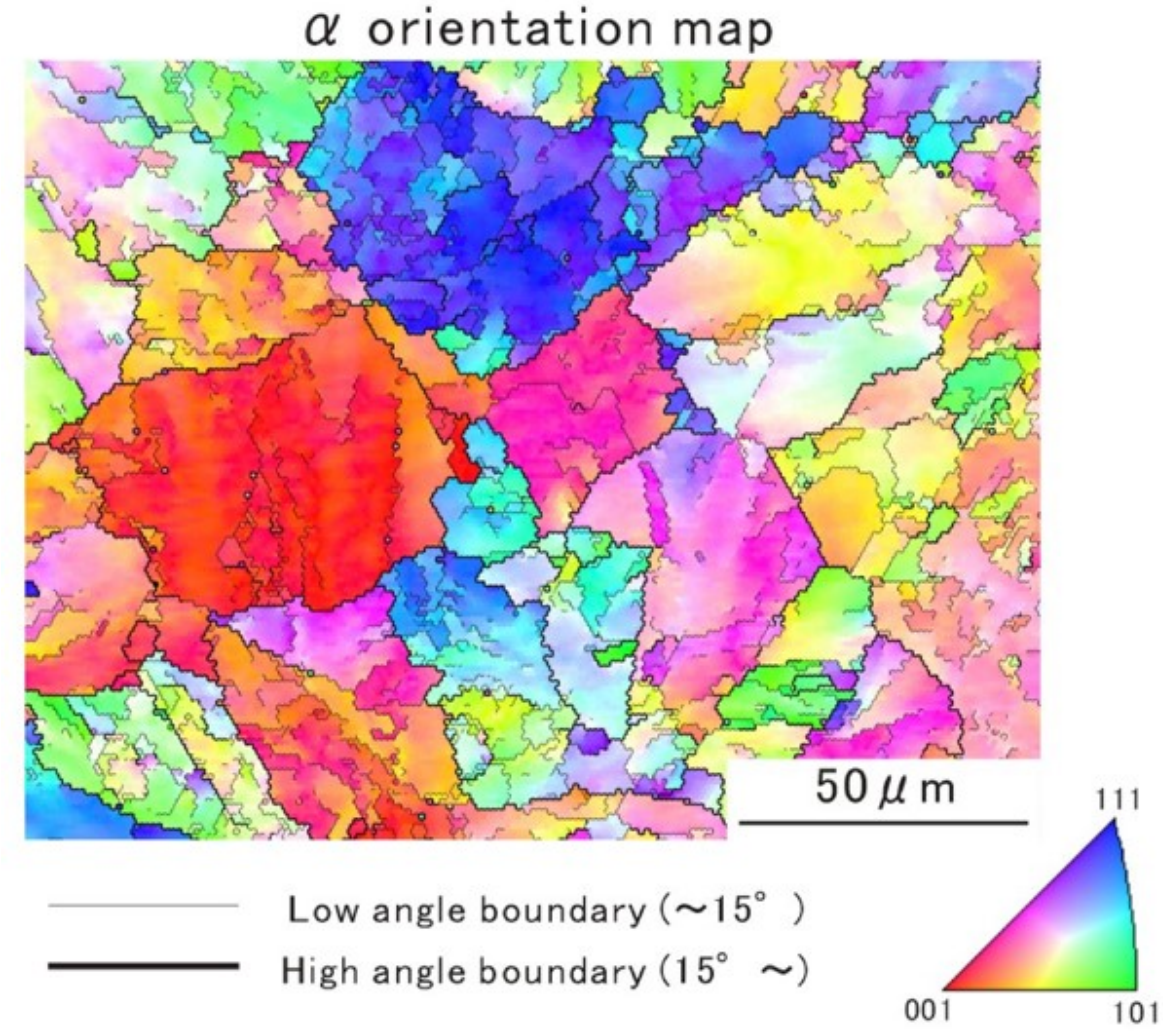

Figure 14: An orientation image of colonies of pearlite (courtesy of S. S. Babu).

The interlamellar spacing within pearlite can be made fine by growing the pearlite at large thermodynamic driving forces. Figure 15 shows a transmission electron micrograph of pearlite where the interlamellar spacing is about 50 nm. This is well below the resolution of an optical microscope (typically 500 nm). It follows that the lamellae in this case cannot be resolved using optical microscopy, as illustrated in Fig. 16.

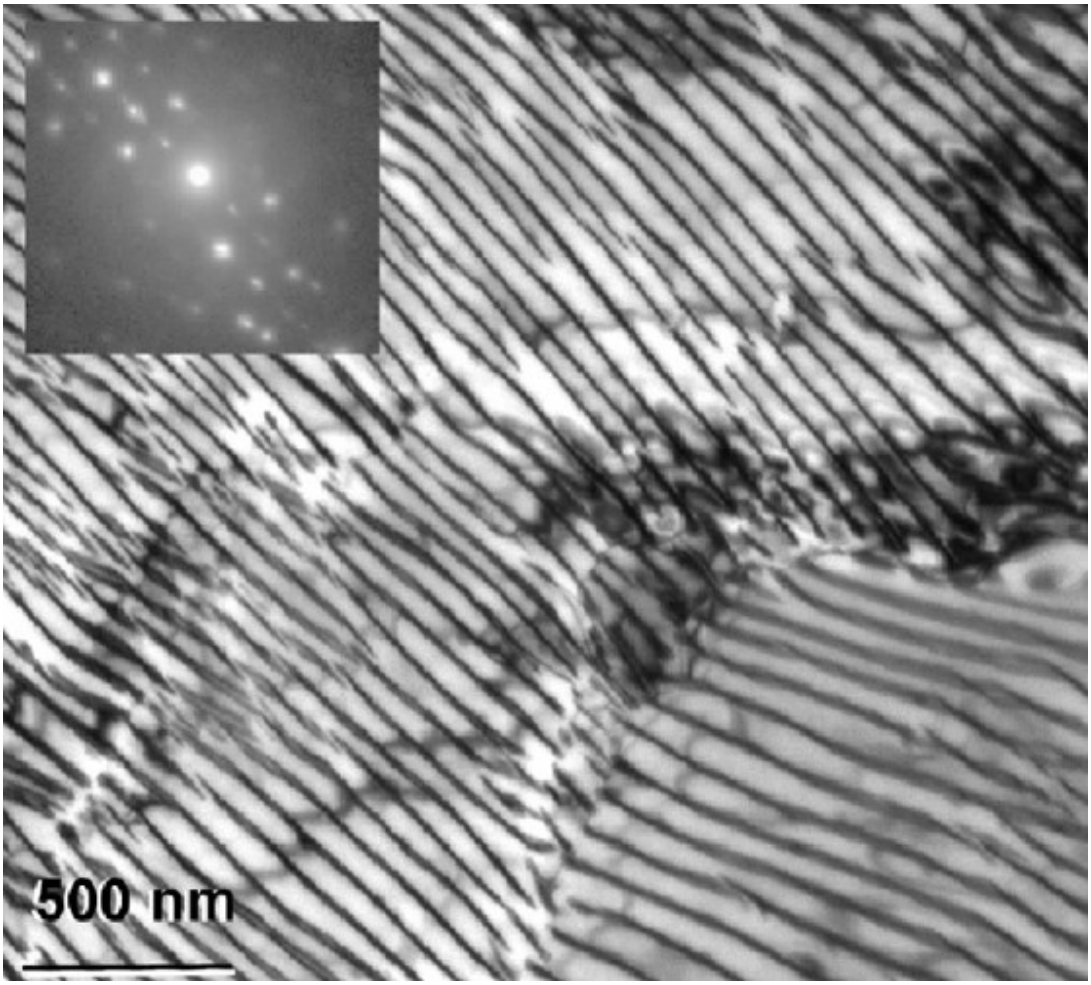

Figure 15: Transmission electron micrograph of extremely fine pearlite.

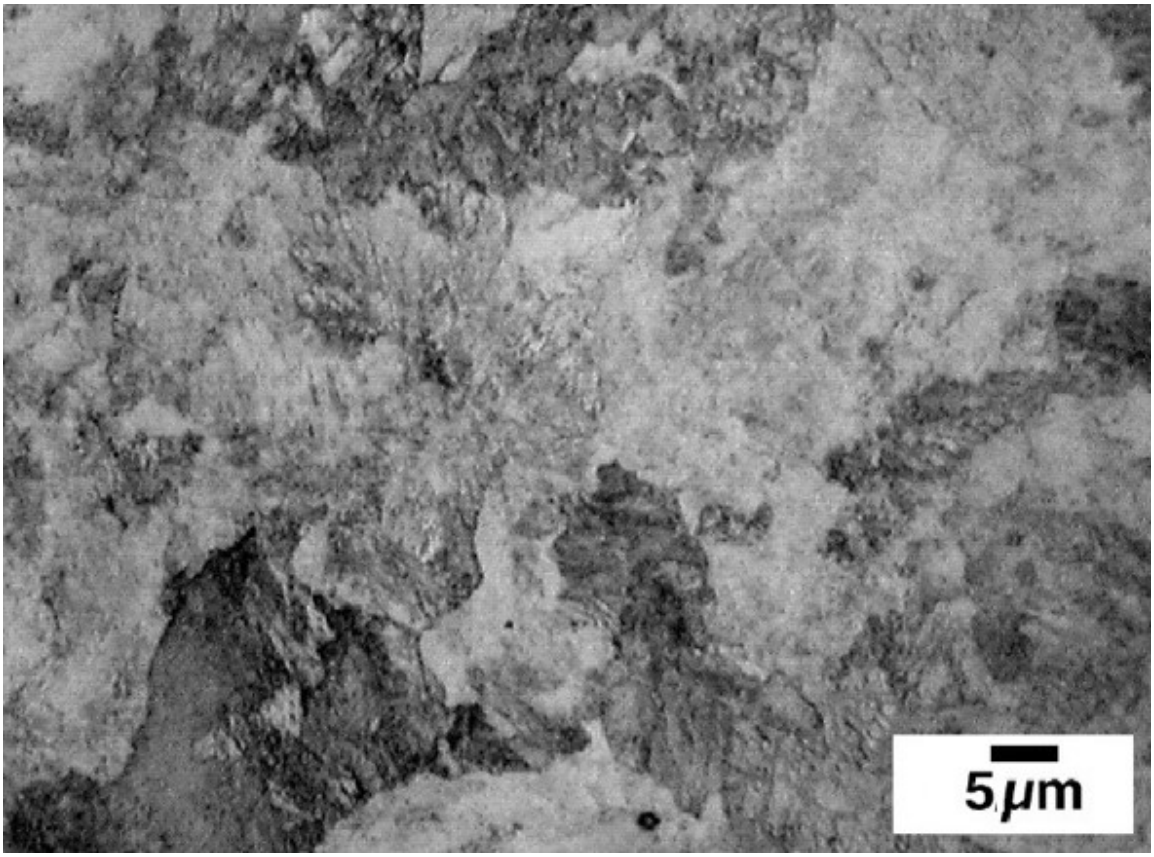

Figure 16: Optical micrograph of extremely fine pearlite from the same sample as used to create Fig. 15. The individual lamellae cannot now be resolved.

Pearlite is a reconstructive transformation which always involves the diffusion of all elements including iron. It cannot happen in the absense of substantial atomic mobility. In alloy steels, in addition to interstitial carbon, the substitutional solutes will partition between the cementite and ferrite. Figure 17 shows this to be the case, with C, Mn and Cr enriching inside the cementite whereas Al and Si partition into the ferrite.

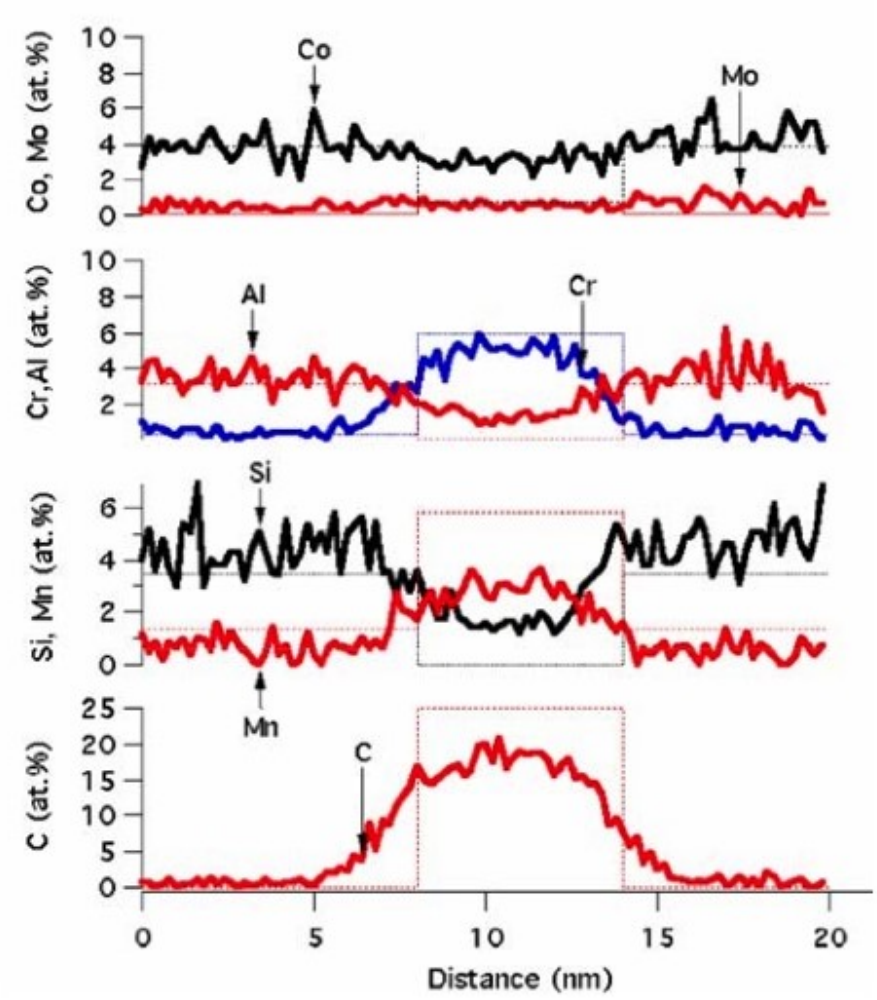

Figure 17: Atom-by-atom chemical analysis across cementite in a pearlite colony (same sample as Figs. 15,16).

It is sometimes the case that a pearlitic steel is too strong for the purposes of machining or other processing. It can then be heat-treated at a temperature below that at which austenite forms, to allow the cementite to *spheroidise*. The "lamellae" of cementite turn into approximately spherical particles of cementite in an effort to minimise the amout of θ/α interfacial area/energy per unit volume (Fig. 18).

Since spheroidisation is driven by interfacial area, fine pearlite spheroidises more readily than coarse pearlite. Plastically deformed pearlite which is fragmented will also spheroidse relatively rapidly (Fig. 19).

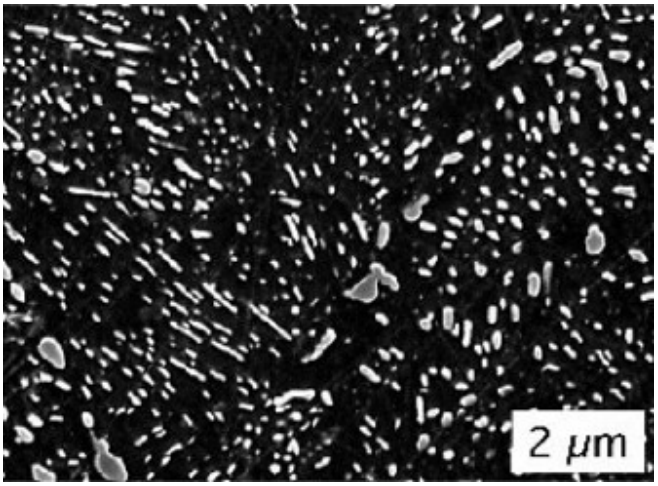

Figure 18: The appearance of an originally pearlitic after a spheroidisation heat treatment at 750°C for 1.5 h (courtesy Ferrer et al., 2005).

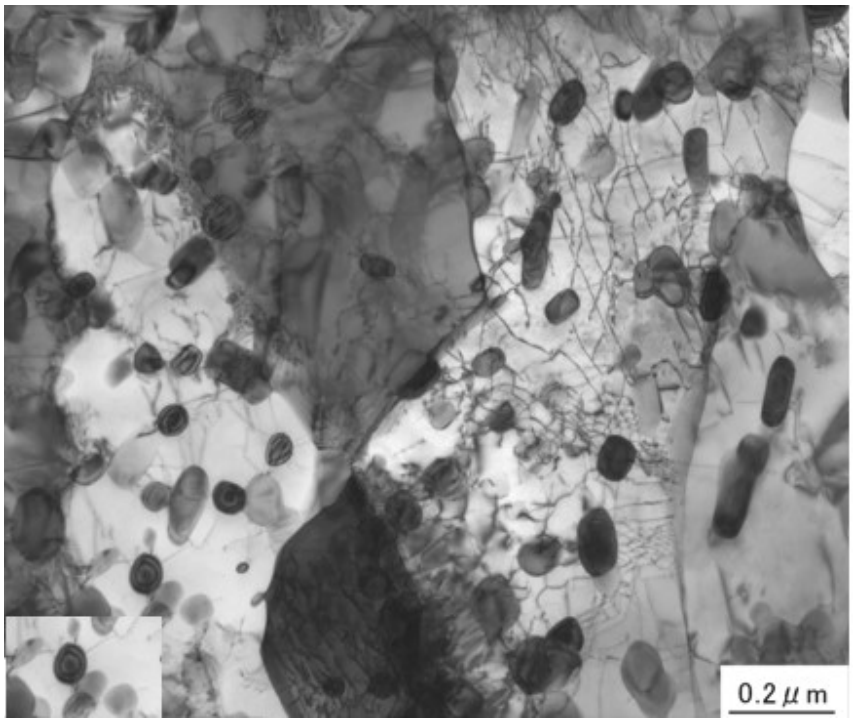

Figure 19: Transmission electron micrograph showing the advanced stages of spheroidisation when plastically deformed pearlite is heat treated at 750°C for 1.5 h (courtesy Ferrer et al., 2005).

The vast majority of commercial steels contain manganese and are produced by casting under conditions which do not correspond to equilibrium. There are as a result, manganese-enriched regions between the dendrites. Any solid-state processing which involves rolling-deformation is then expected to smear these enriched regions along the rolling direction, thus building into the steel *bands* of Mn-enriched and Mn-depleted regions.

When the austenite in such steels is cooled, ferrite first forms in the Mn-depleted regions. Ferrite has a very low solubility for carbon which partitions into the Mn-enriched regions which on further cooling, transform into bands of pearlite. The banded

microstructure is illustrated in Fig. 20. Fig. 21 shows microanalysis data which confirm that pearlite tends to form in the Mn-enriched regions.

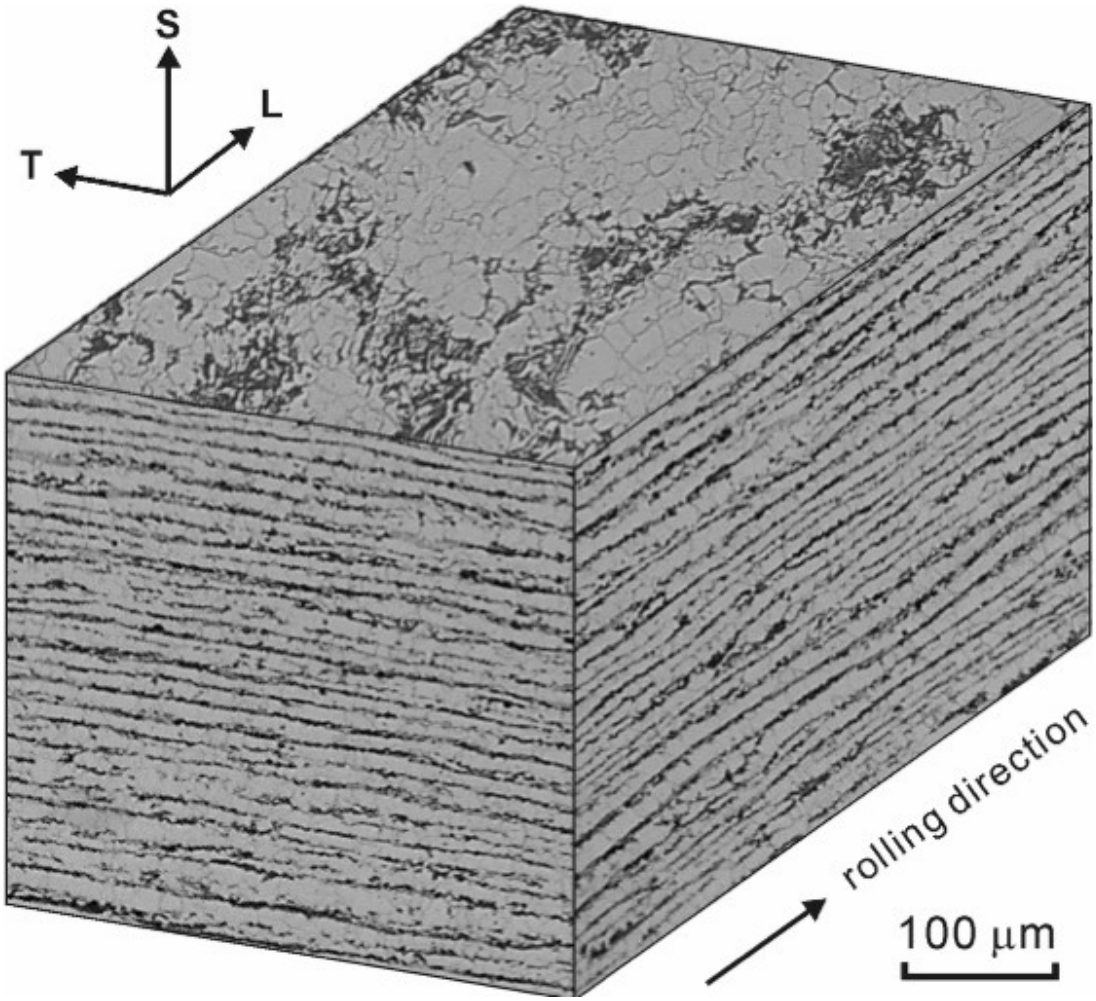

Figure 20: Banded microstructure (courtesy ****)
"T", "L" and "S" stand for transverse, longitudinal and short-transverse directions respectively.

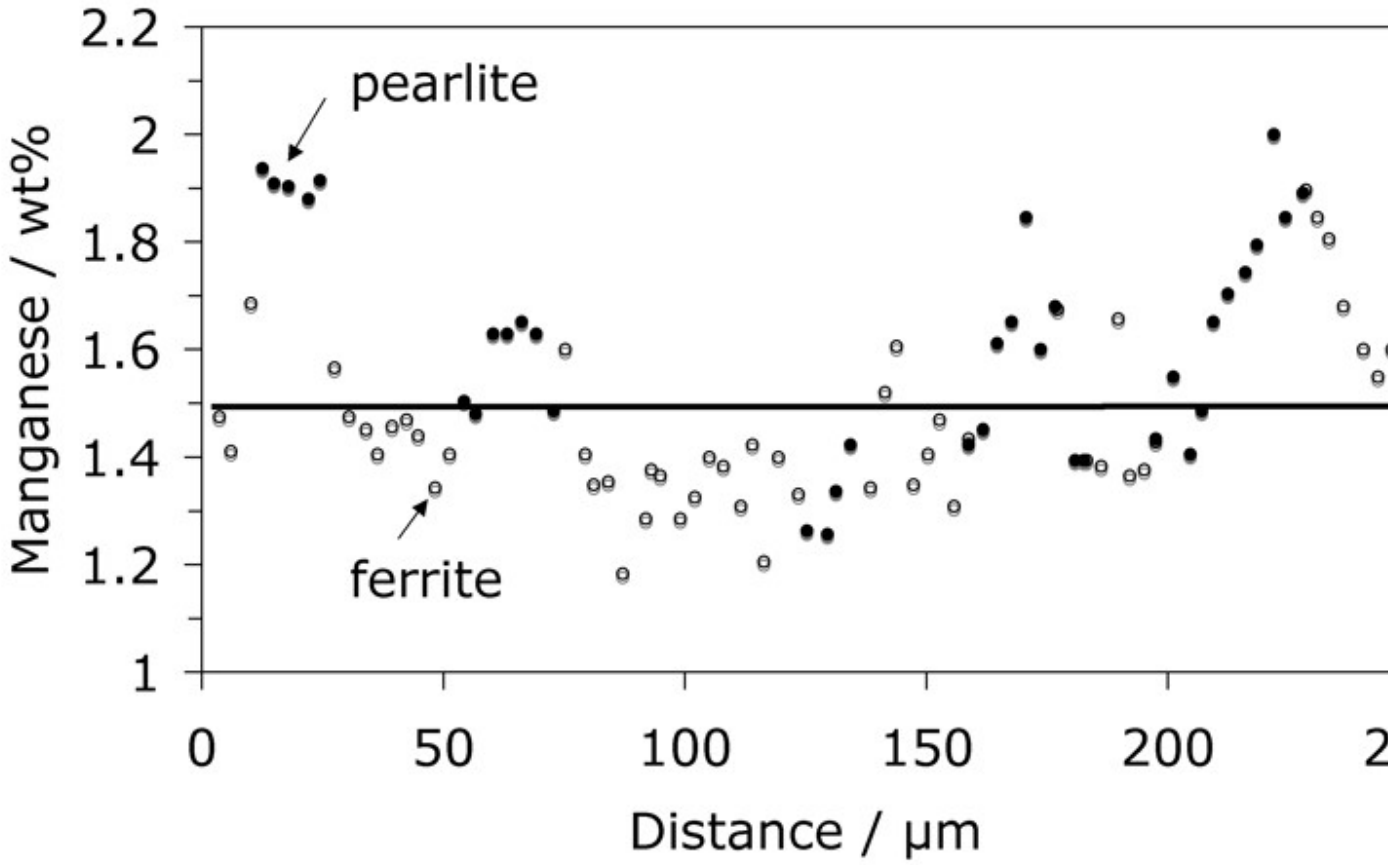

Figure 21: Showing that the manganese depleted regions correspond to ferrite whereas those which are enriched transform into pearlite (courtesy of Howell).

Martensite

Martensite transformation begins when austenite is cooled to a temperature below M_S on the time-temperature-transformation diagram. It is a diffusionless transformation achieved by the deformation of the parent lattice into that of the product.

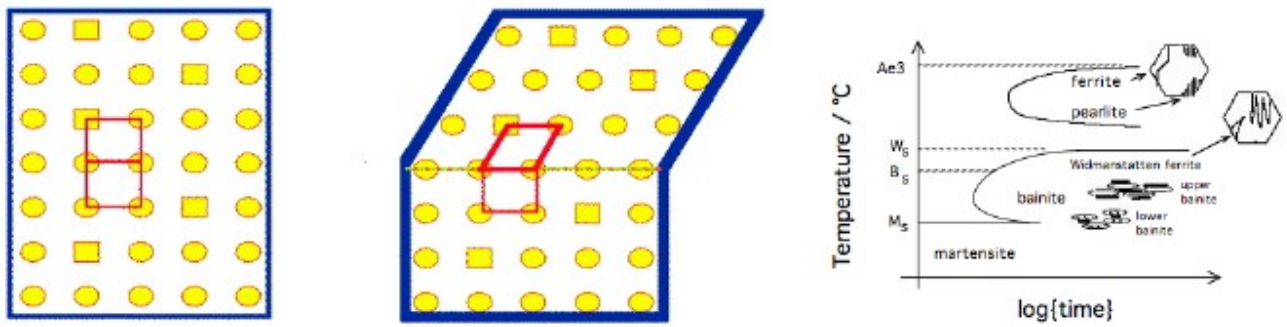

Figure 22: Mechanism of martensitic transformation and the martensite-start temperature.

Fig. 23 shows an interference micrograph of a sample of austenite which was polished flat and then allowed to transform into martensite. The different colours indicate the displacements caused when martensite forms. This physical deformation is described on a macroscopic scale as an *invariant-plane strain* (Fig. 24) consisting of a shear strain *s* of about 0.25 and a dilatation δ normal to the habit plane of about 0.03.

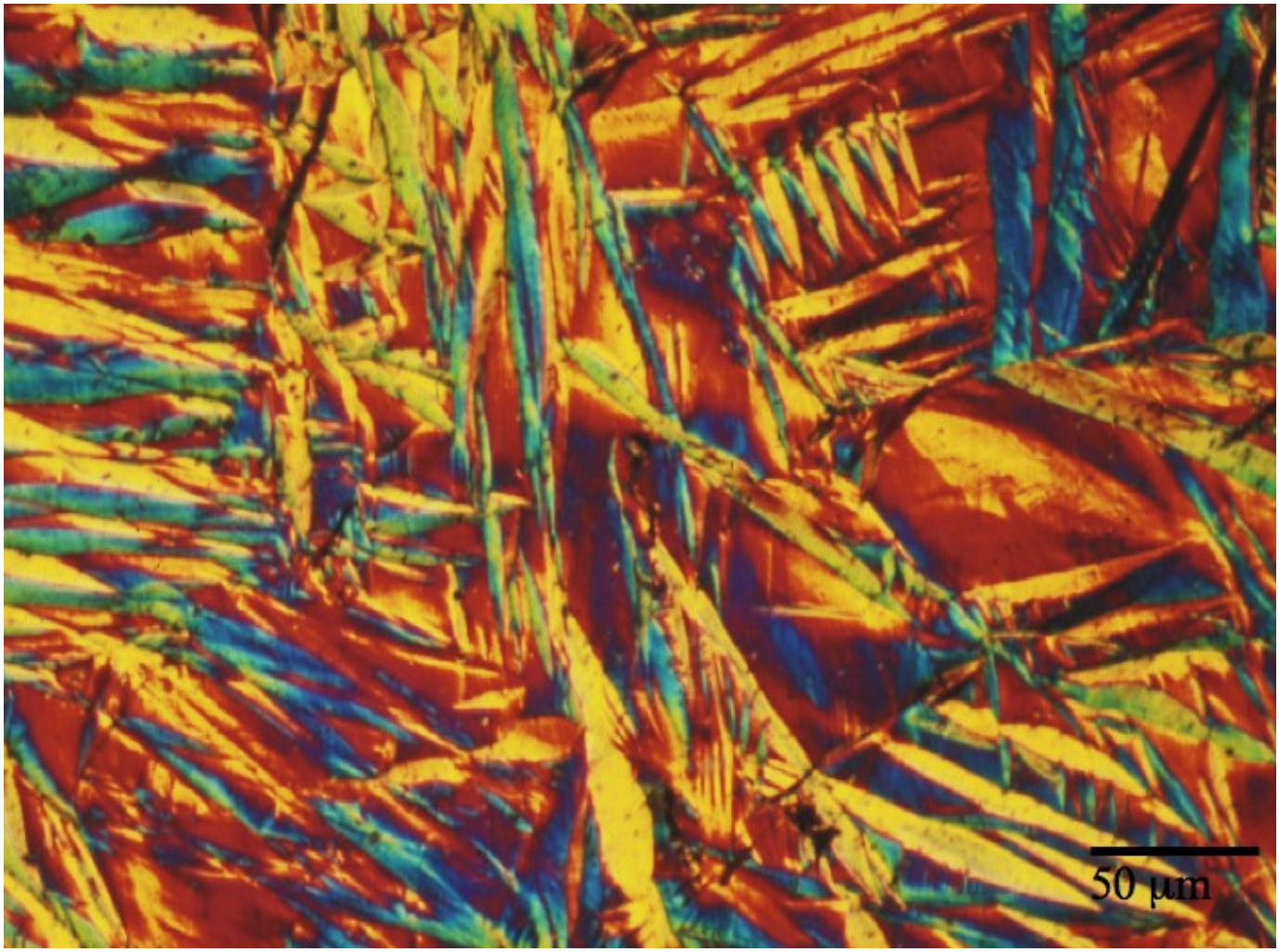

Figure 23: Nomarski intereference micrograph showing the surface displacements accompanying martensitic transformation.

The strain energy per unit volume, *E* scales with the shear modulus of the austenite µ the strains and the thickness to length ratio *c/r* as illustrated in Fig. 24. The martensite therefore forms as a thin plate in order to minimise the strain energy. All of the displacive transformation products are therefore in the form of thin plates.

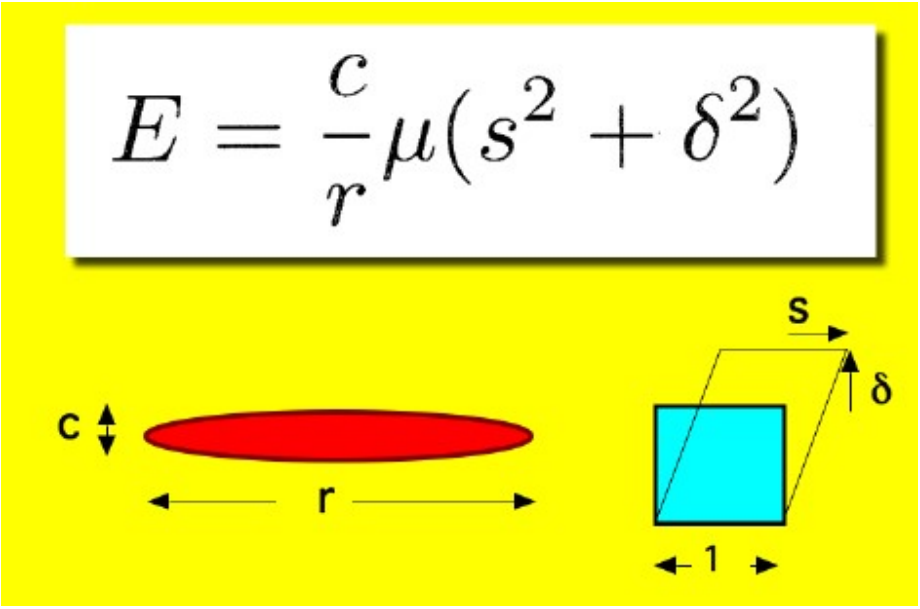

Figure 24: Mechanism of martensitic transformation and the martensite-start temperature.

We have emphasised that the discipline motion of atoms cannot be sustained across austenite grain boundaries and hence plates of martensite, unlike allotriomorphs, are confined to the grains in which they nucleate (Fig. 25).

The austenite grain boundaries are thus destroyed in the process of forming allotriomorphic ferrite or pearlite. This is not the case with displacive transformation products where even if all the austenite is consumed, a vestige of the boundary is left as the *prior austenite grain boundary*. Austenite grain boundaries and indeed, prior austenite grain boundaries, absorb detrimental impurities. One consequence is that strong steels based on microstructures obtained by displacive transformation become susceptible to impurity embrittlement.

Fig. 26 shows the form of the fracture surface expected when failure occurs due to impurity embrittlement at the prior austenite grain boundaries. The grains simply separate at the grain surfaces with little absorption of energy during fracture.

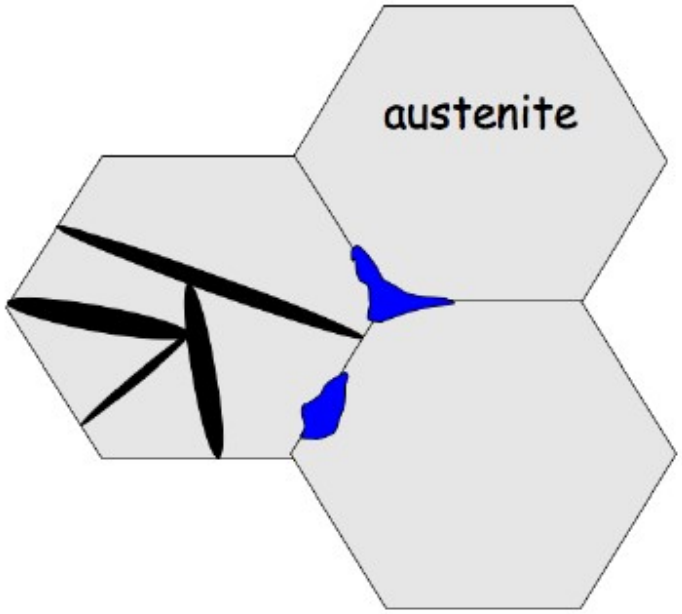

Figure 25: Whereas allotriomorphs can grow across grains, plates of martensite are confined within the grain in which they nucleate.

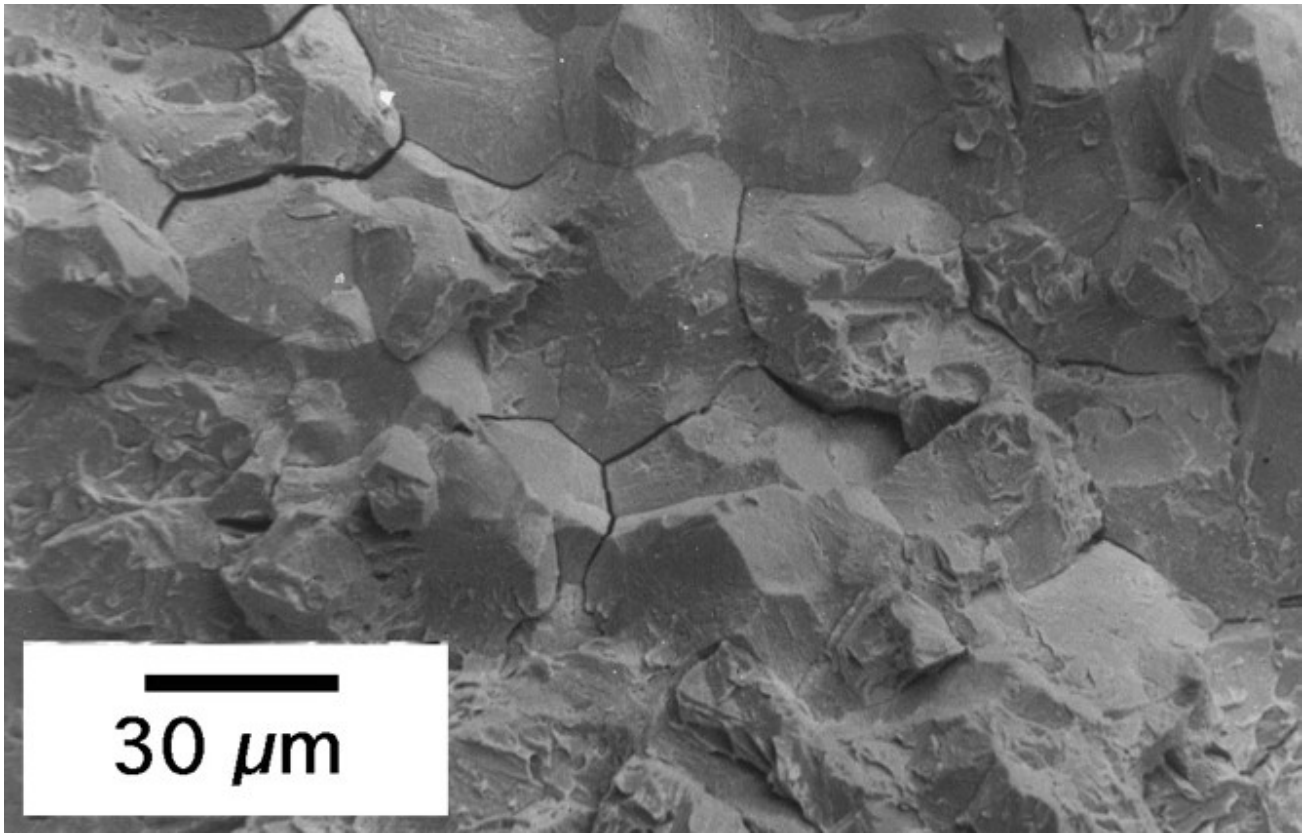

Figure 26: Scanning electron micrograph showing failure of a bainitic steel through embrittlement of the prior austenite grain boundaries.

In alloys containing large concentrations of solutes (for example, Fe-1C wt% or Fe-30Ni wt%), the plate shape of martensite is clearly revealed because substantial amounts of retained austenite are present in the microstructure, as illustrated in Fig. 27. In contrast, lower alloy steels transform almost completely to martensite when cooled sufficiently rapidly. Therefore, the microstructure appears different (Fig. 28) but still consists of plates or laths of martensite.

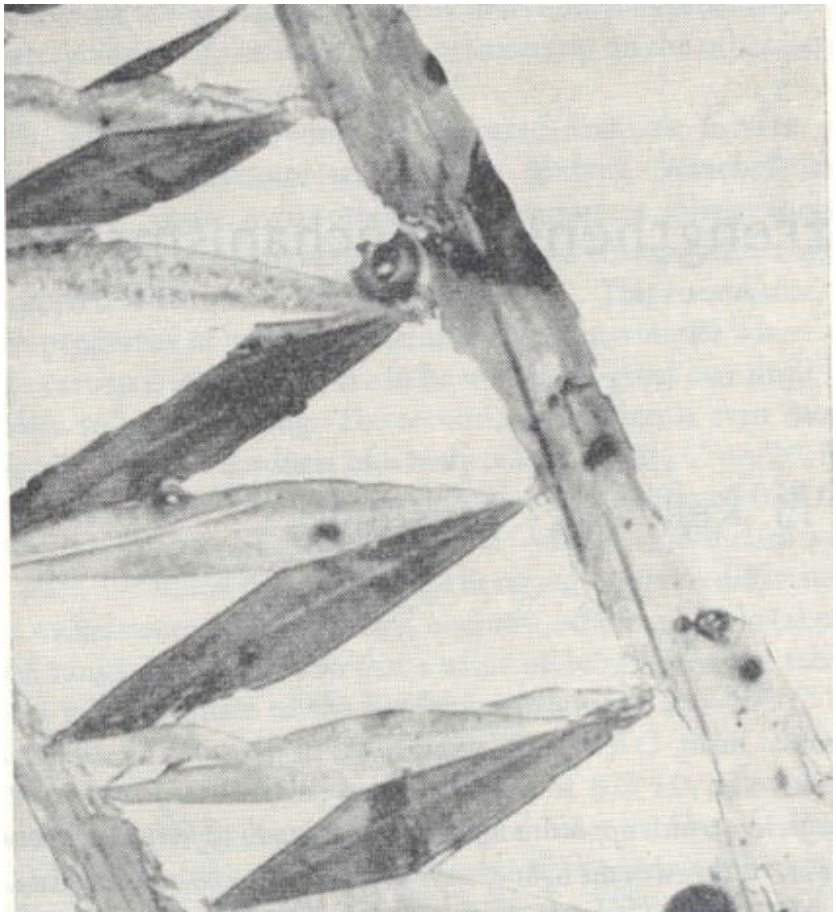

Figure 27: Plates of martensite in an alloy which is rich in nickel.

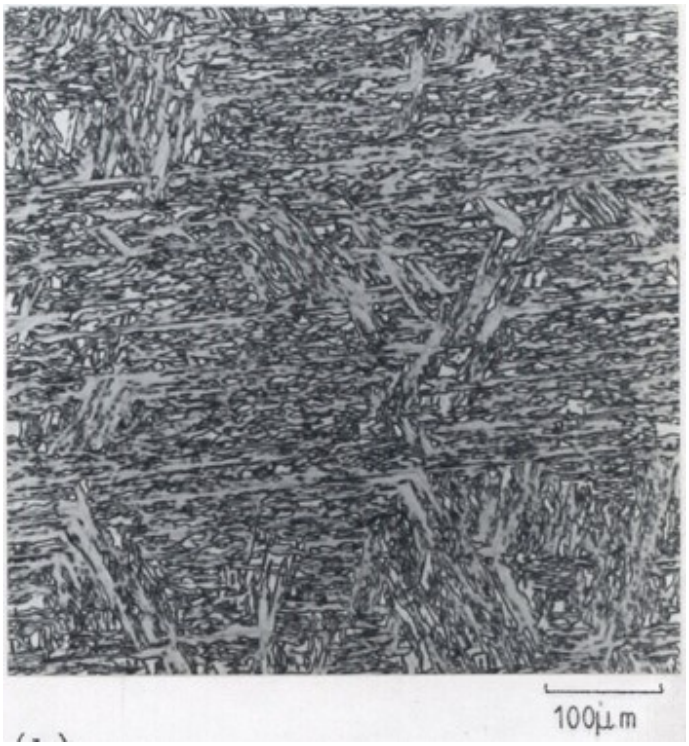

Figure 28: Martensite in a low-alloy steel.

Transmission electron microscopy can reveal the small amount of inter-plate retained austenite in low-alloy steels (Fig. 29).

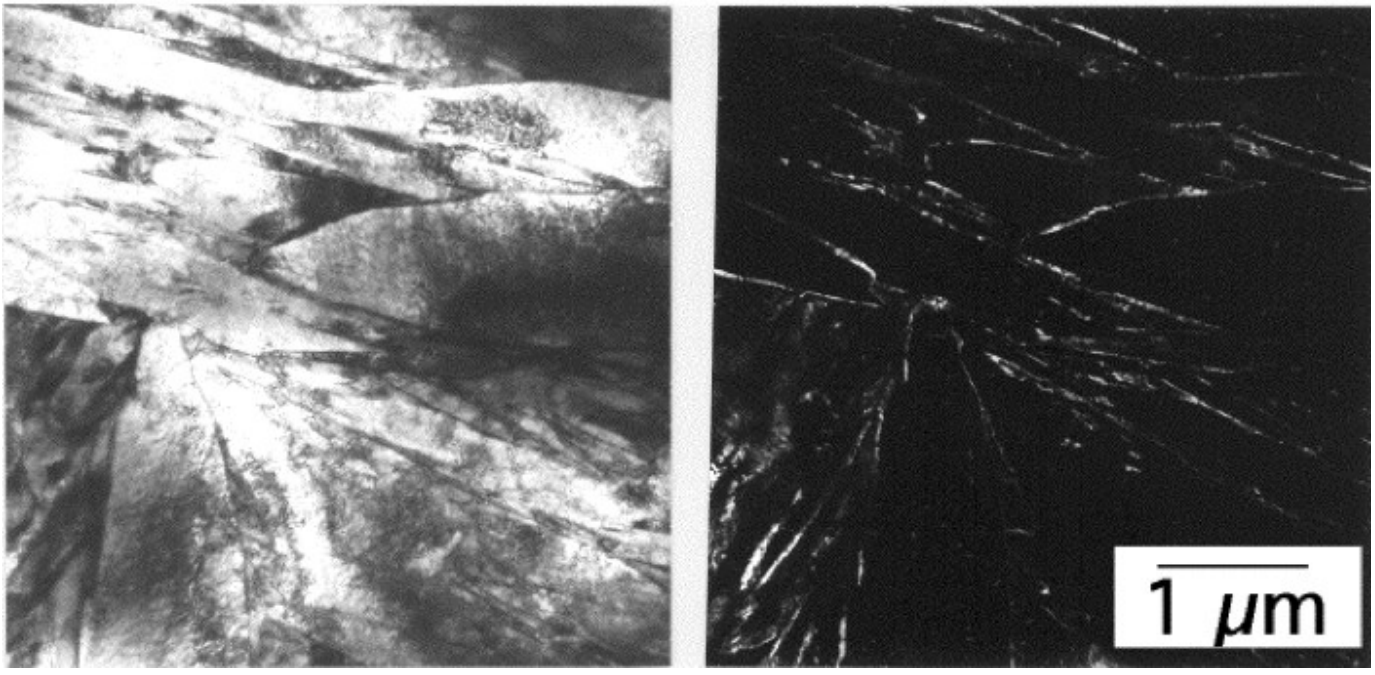

Figure 29: (a) Transmission electron micrograph of as-quenched martensite in a Fe-4Mo-0.2C wt% steel. The mottled contrast within the plates is due to a high density of dislocations. (b) Corresponding dark-field image showing the distribution of retained austenite.

Tempering at a low temperature relieves the excess carbon trapped in the martensite, by the precipitation of cementite. The retained austenite is not affected by tempering at temperatures below M_S, Fig. 30.

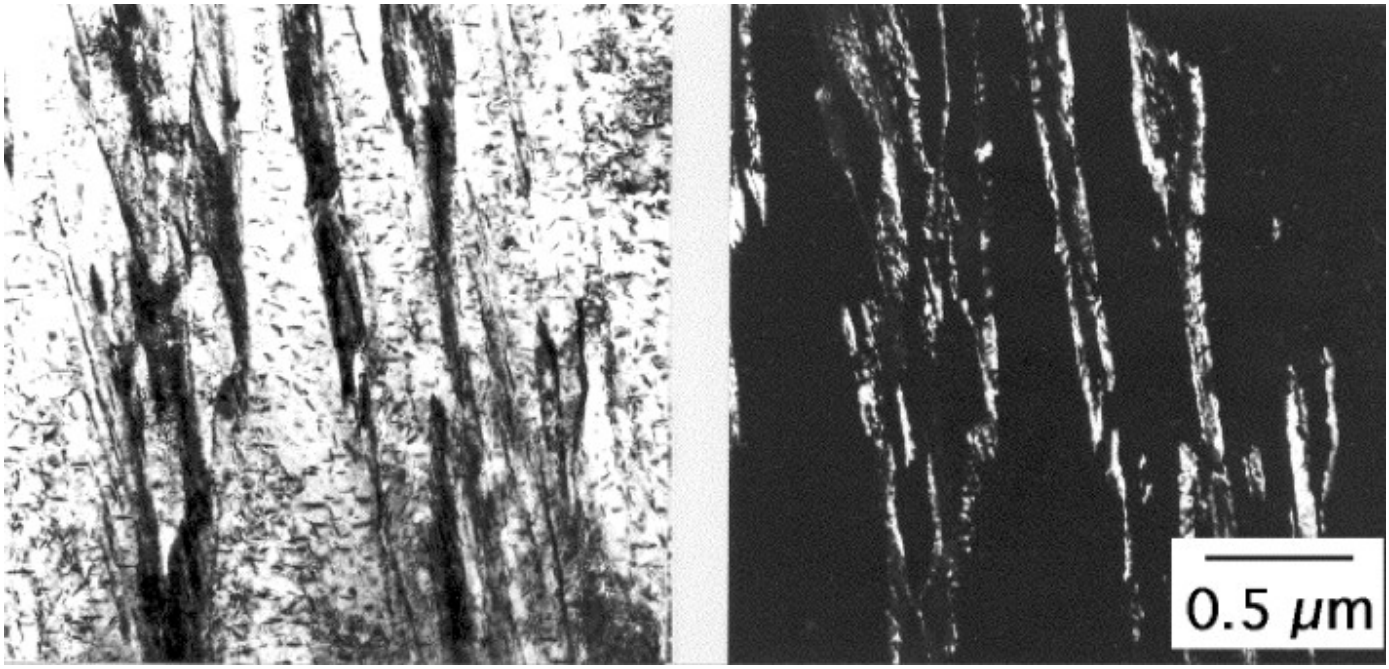

Figure 30: (a) Transmission electron micrograph of martensite in a Fe-4Mo-0.2C wt% steel after tempering at 190°C for 1 hour. The carbon has in this case precipitated as fine particles of cementite. (b) Corresponding dark-field image showing the distribution of retained austenite, which has not been affected by the tempering.

In some steels containing a strong carbide-forming elements such as Mo or V, tempering at temperatures where these solutes are mobile leads to the precipitation of alloy carbides (Fig. 31).

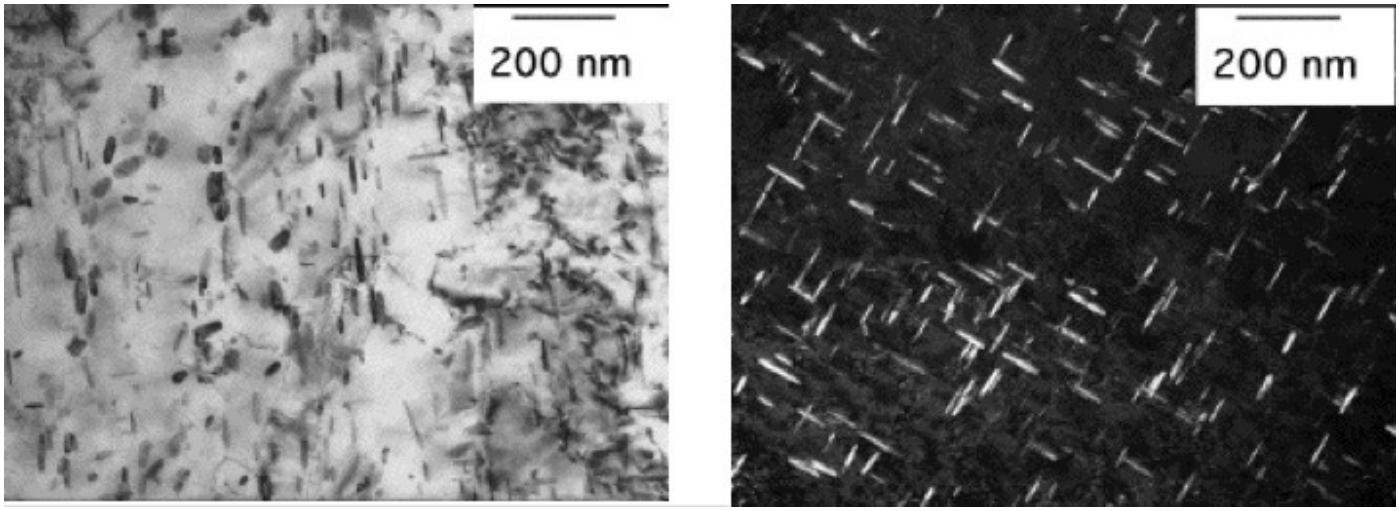

Figure 31: Fe-0.1C-1.99Mn-1.6Mo wt% quenched to martensite and then tempered at 600°C. (photograph courtesy of Shingo Yamasaki). The bright field transmission electron micrograph is of a sample tempered for 560 h, whereas the dark-field image shows a sample tempered for 100 h. The precipitates are needles of Mo_2C particles. The needles precipitate with their long directions along $<100>_{\alpha}$.

The Bain strain which converts austenite into martensite is a huge deformation; to mitigate its effects there are other deformations which accompany the transformation. These change the overall shape deformation into an invariant-plane strain. One consequence is that there are lattice invariant deformations such as slip and twinning on a fine scale. Slip simply leads to steps in the interface, whereas twinning also introduces interfaces inside the martensite plate, as illustrated in Fig. 32.

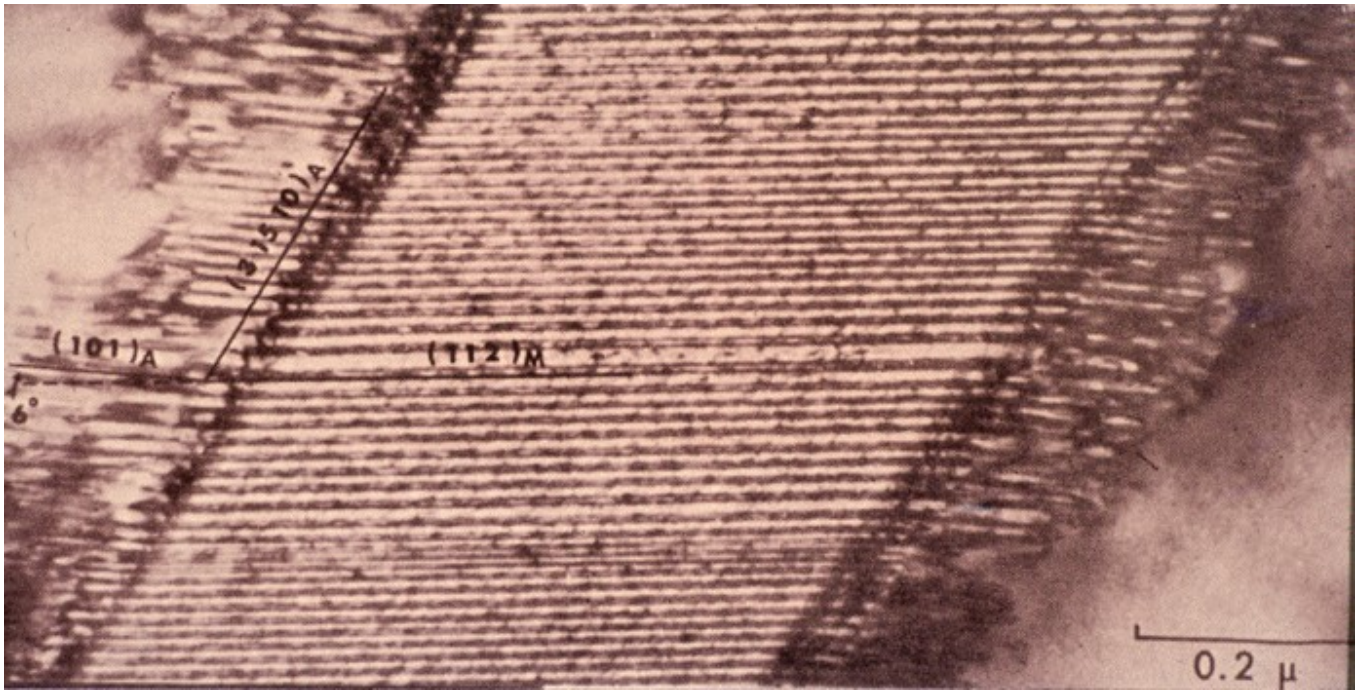

Figure 32: Transformation twins in a plate of martensite (courtesy T. Maki).

Bainite

The atomic mechanism of bainite is similar to that of martensite (Fig. 33). Plates of bainite form without any diffusion, but shortly after transformation, the carbon partitions into the residual austenite and precipitates as cementite between the ferrite platelets - this is the structure of upper bainite (Fig. 34). Lower bainite is obtained by transformation at a lower temperature; the carbon partitioning is then slower, so some of the excess carbon has an opportunity to precipitate inside the ferrite plates and the rest of it precipitates from the carbon-enriched austenite as in upper bainite, Fig. 34.

The difference between bainite and martensite is at primarily at the nucleation stage. Martensitic nucleation is diffusionless, but it is thermodynamically necessary for carbon to partition during the nucleation of bainite. Bainite also forms at temperatures where the austenite is mechanically weak. The shape deformation due to the bainite transformation is therefore casues plastic deformation in the adjacent austenite. This deformation stops the bainite plates from growing and transformation then proceeds by the nucleation of further plates, which also grow to a limited size.

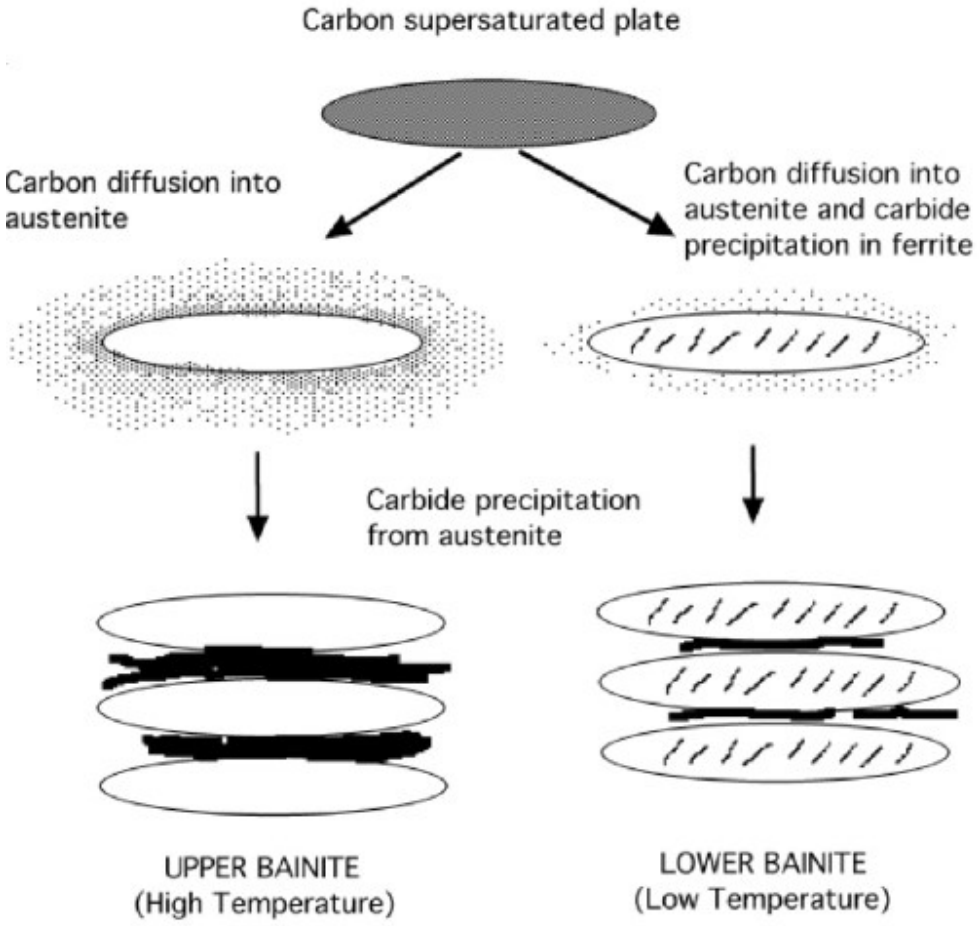

Figure 33: Summary of the mechanism of the bainite reaction.

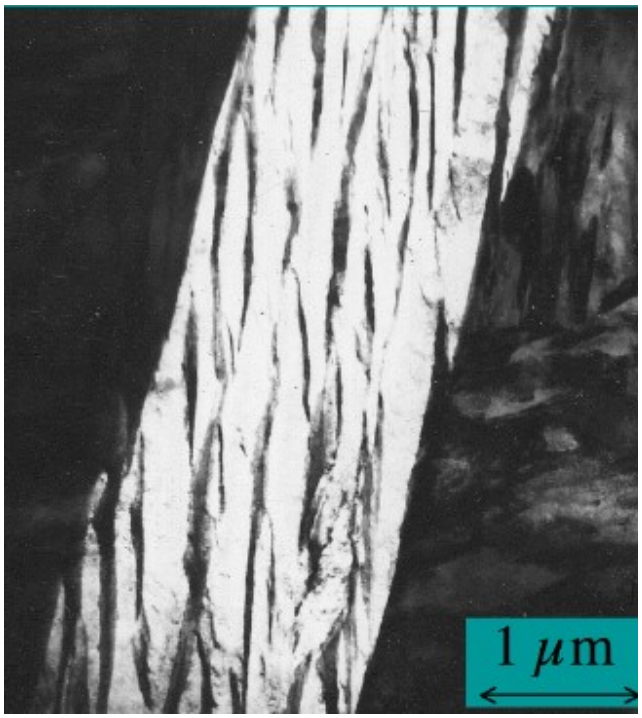

Figure 34: Upper bainite; the phase between the platelets of bainitic ferrite is usually cementite.

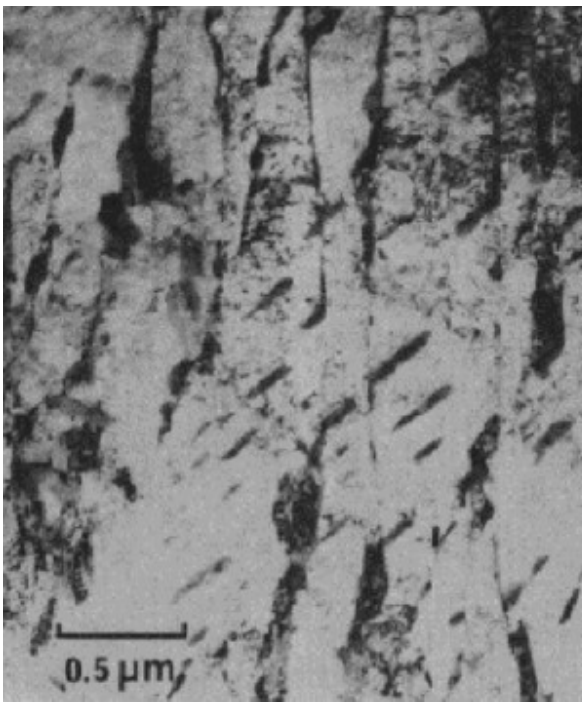

Figure 35: Lower bainite, with cementite inside the platelets and also between the platelets of bainitic ferrite.

Widmanstätten Ferrite

We have categorised transformations into displacive and reconstructive, with the former being strain dominated and the latter diffusion dominated. Displacive transformations are also known as *military* transformations by analogy to a queue of solidiers boarding a bus. The soliders board the bus in a disciplined manner such that there is a defined correspondence between their positions in the bus and those in the queue. Near neighbours remain so on boarding. There is thus no diffusional mixing and no composition change. Because the soldiers are forced to sit in particular positions, there will be a lot of strain energy and this is not an equilibrium scenario.

A *civilian* transformation is one in which the queue of civilians board the bus in an un-coordinated manner so that all correspondence between the positions in the bus and the queue is lost. Civilians occupy the positions they prefer to occupy, a situation analogous to diffusion.

There is a third kind of transformation, *paraequilibrium* in which the larger atoms in substitutional sites move in a discipline manner (without diffusion) whereas the faster moving interstitial atoms diffuse and partition between the phases. This is how

Widmanstätten ferrite grows, a displacive mechanism whose rate is controlled by the diffusion of carbon in the austenite ahead of the α_w/γ interface.

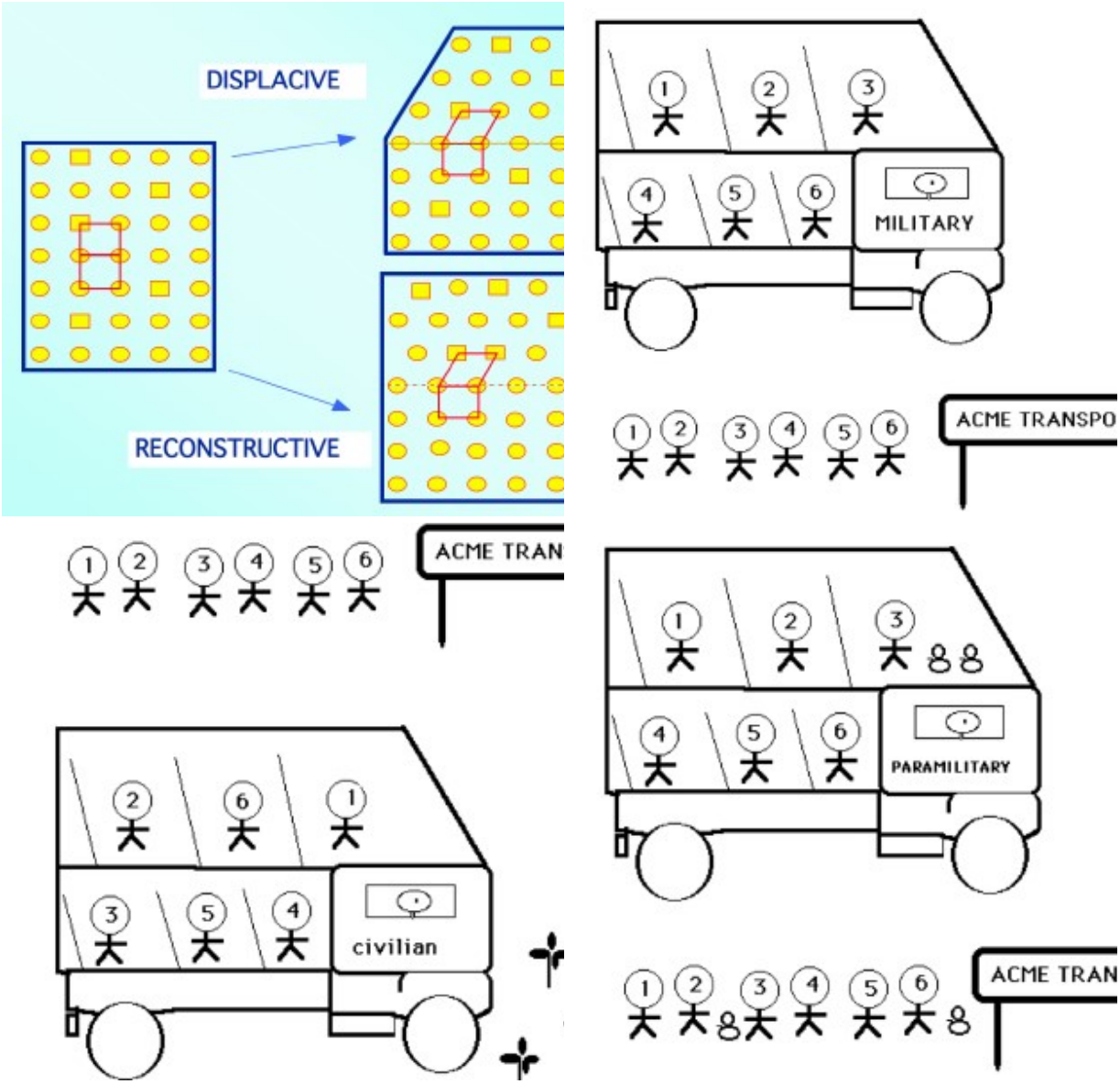

Figure 36: Analogies to the three of the atomic mechanisms of solid-state transformation in steels.

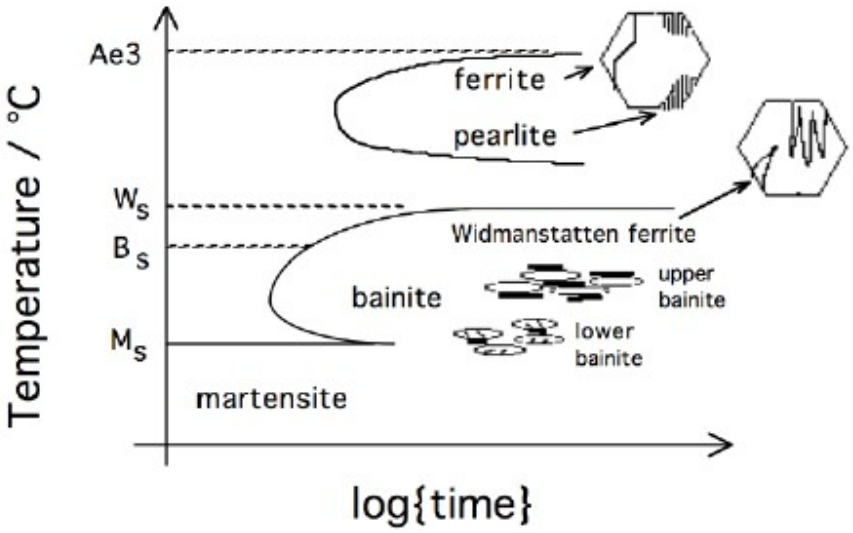

Figure 37: Widmanstätten ferrite on the time-temperature-transformation diagram

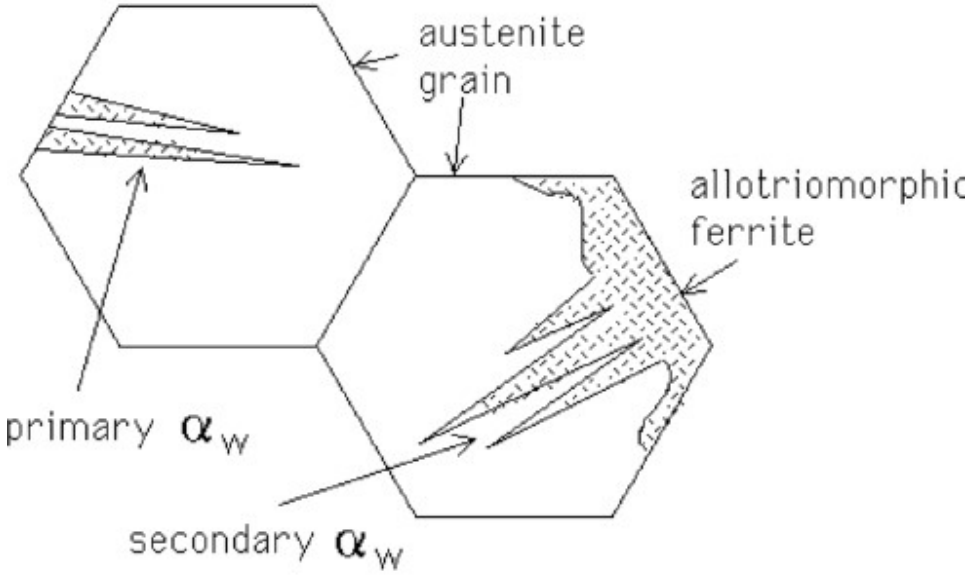

Figure 38: Schematic illustration of primary Widmanstätten ferrite which originates directly from the austenite grain surfaces, and secondary α_w which grows from allotriomorphs.

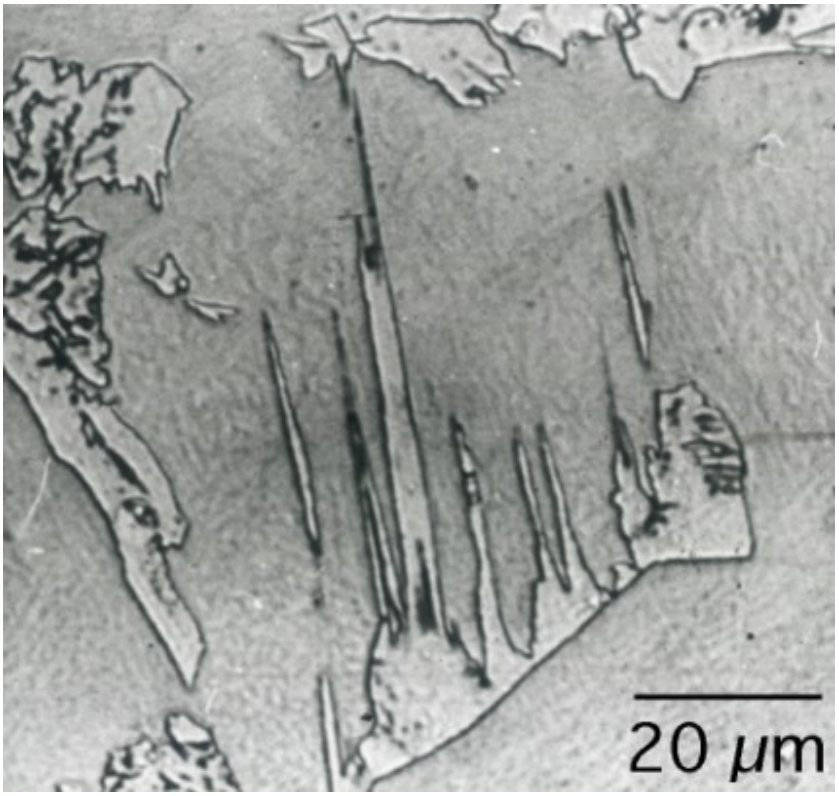

Figure 39: Optical micrographs showing white-etching (nital) wedge-shaped Widmanstätten ferrite plates in a matrix quenched to martensite. The plates are coarse (notice the sacle) and etch cleanly because they contain very little substructure.

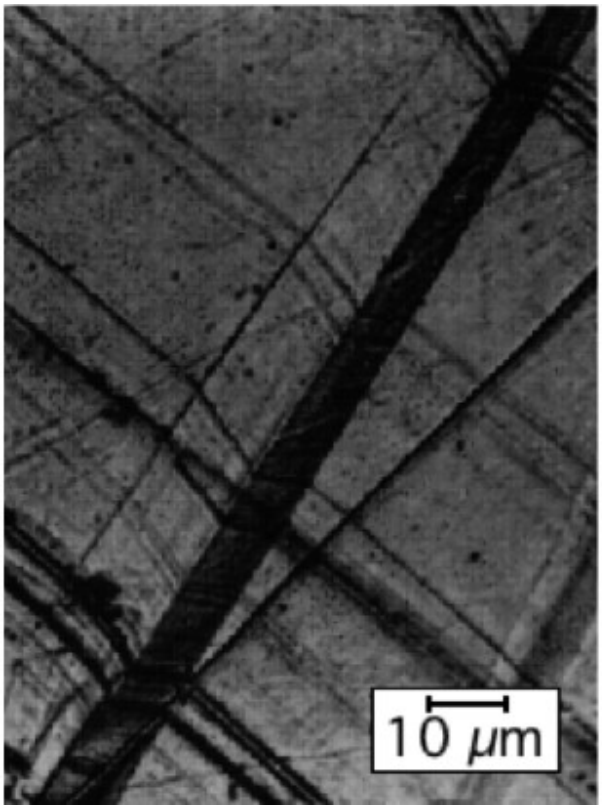

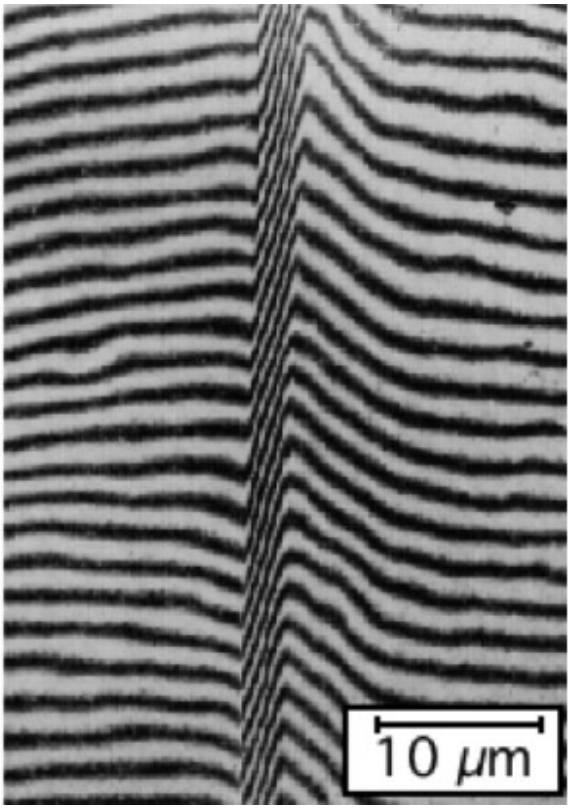

Figure 40: After Watson and McDougall. Shows the displacements caused by the growth of Widmanstätten ferrite plates. The sample was polished, austenitised and then transformed. The deflection of scratches is evident on the left, and that of Tolansky interference fringes on the right. Notice that the surface relief due to transformation is in the shape of a tent rather than a single invariant-plane strain.

In fact, the strain energy due to the shape deformation when an individual plate of Widmanstätten ferrite forms is generally so high that it cannot be tolerated at the low driving-force where it grows. As a consequence, two back-to-back plates which accommodated each others shape deformation grow simultaneously. This dramatically reduces the strain energy, but requires the simultaneous nucleation of appropriate crystallographic variants. As a consequence, the probablity of nucleation is reduces and the microstructure is coarse. The characteristic thin-wedge shape of α_w is because the two component plates have different habit plane variants with the parent austenite.

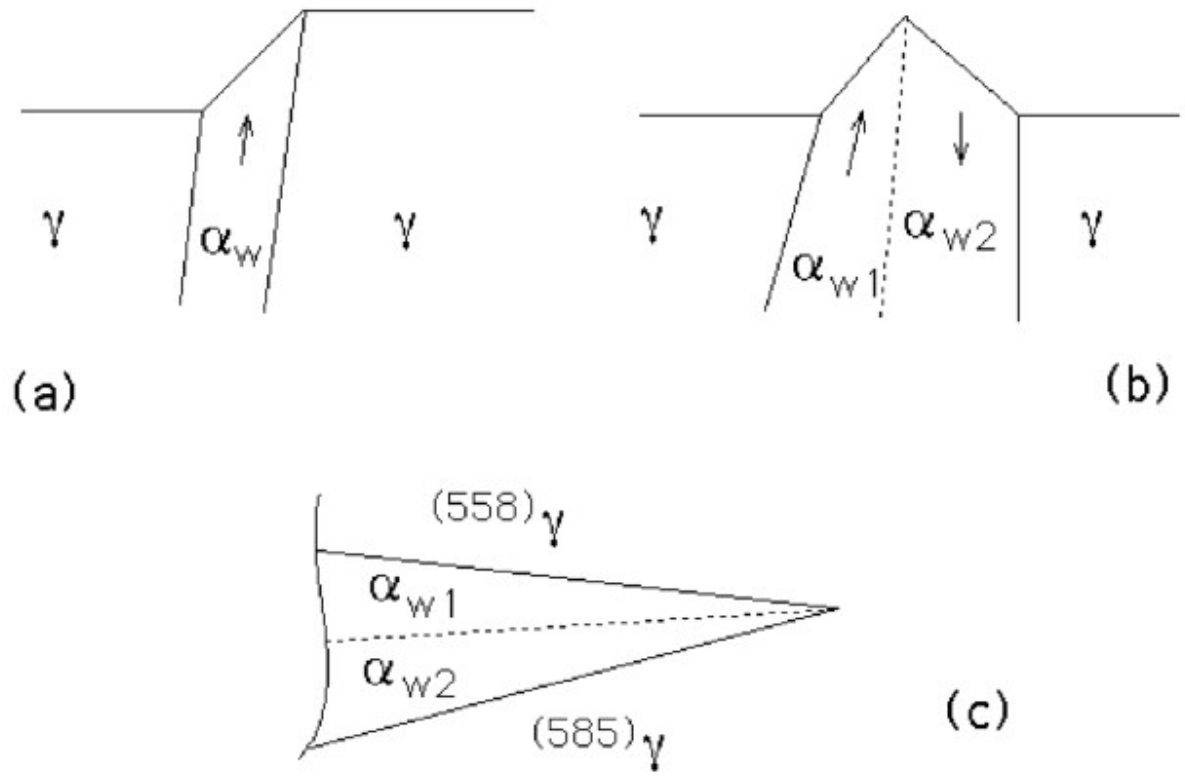

Figure 41: The simultaneous growth of two self-accommodating paltes and the consequential tent-like surface relief.

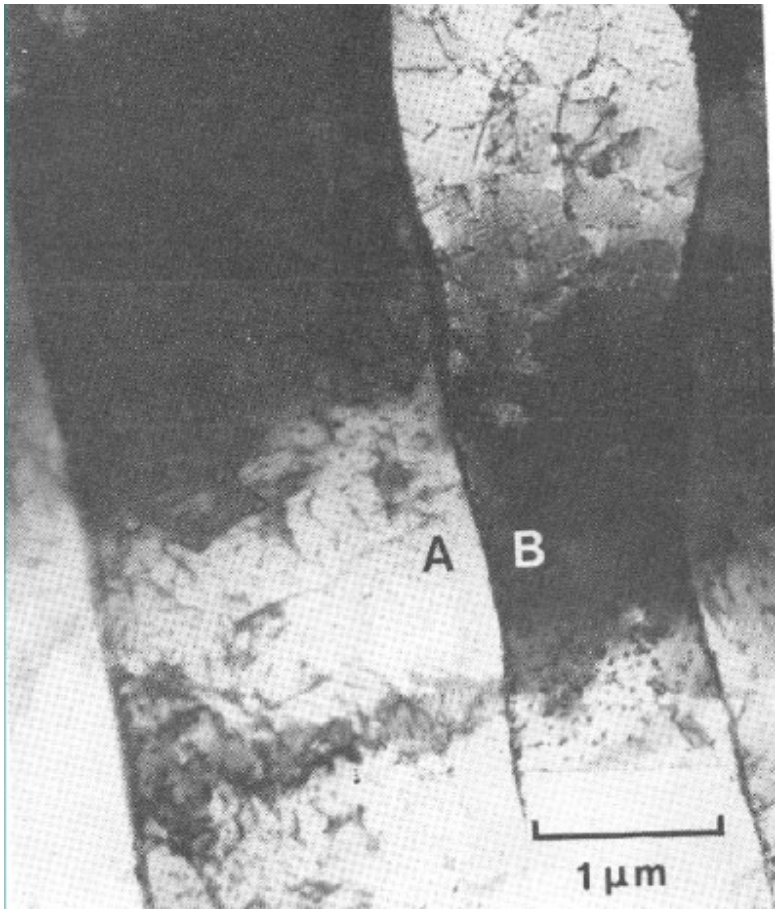

Figure 42: Transmission electron micrograph of what optically appears to be single plate, but is in fact two mutually accommodating plates with a low-angle grain boundary separating them.

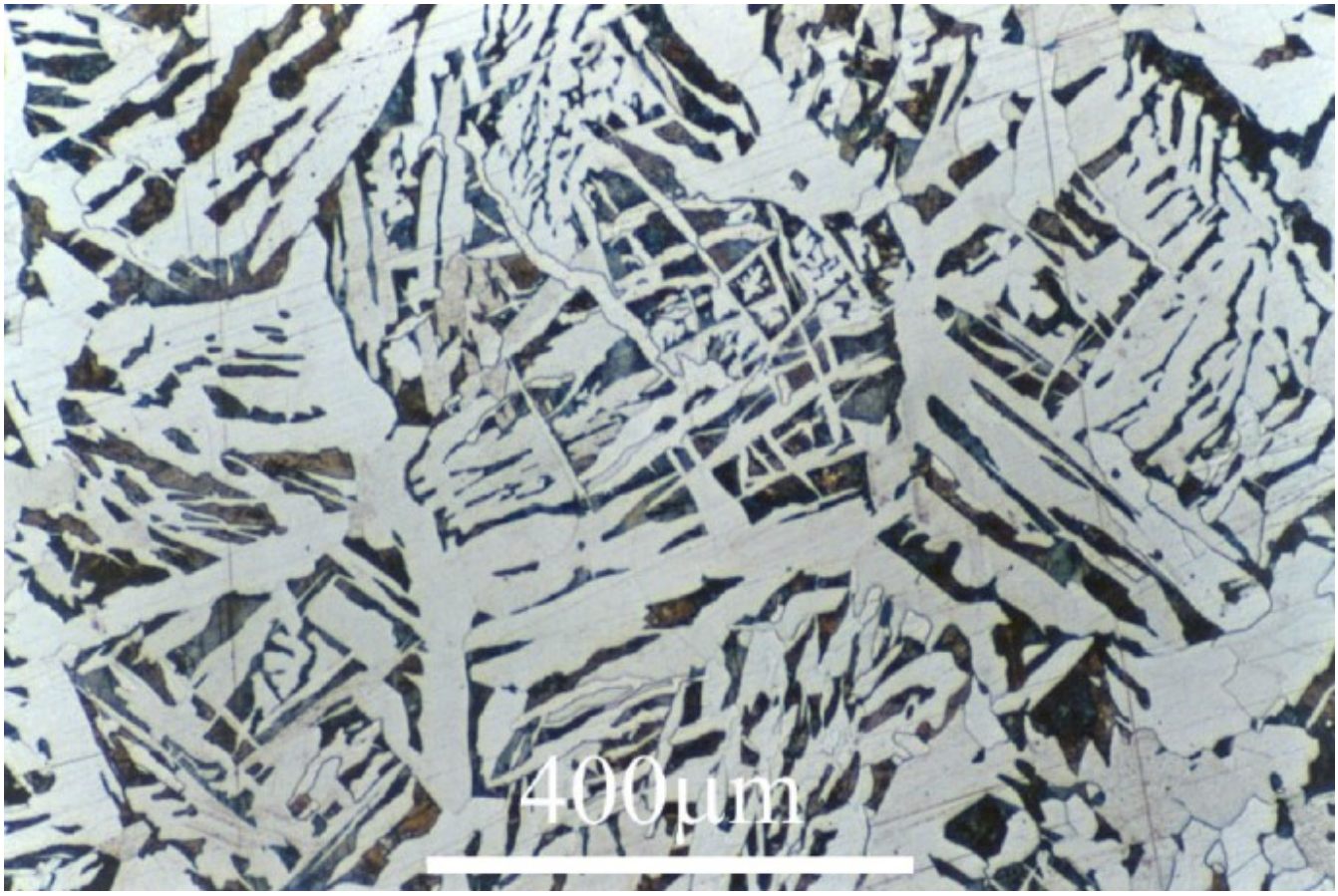

Figure 43: Mixture of allotriomorphic ferrite, Widmanstätten ferrite and pearlite. Micrograph courtesy of DoItPoms project.

Mixed Microstructures

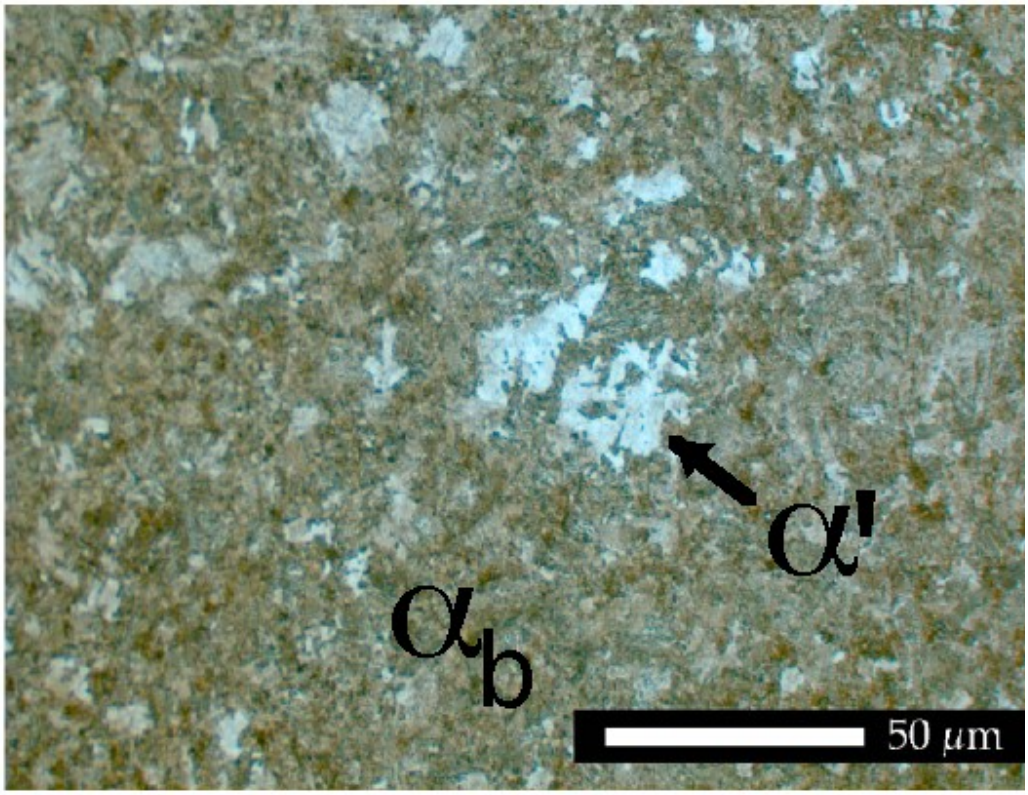

Figure 44: Optical micrograph of a mixed microstructure of bainite and martensite in a medium carbon steel. The bainite etched dark because it is a mixture of ferrite and cementite, and the α_b/θ interfaces are easily attacked by the nital etchant used. The residual phase is untempered martensite which etches lighter because of the absence of carbide precipitates.

It is follows that it is easy, using optical microscopy, to distinguish bainite and martensite as long as both phases are presente in the microstructure. This is even though optical microscopy cannot resolve the detailed structure described in Fig. 34.

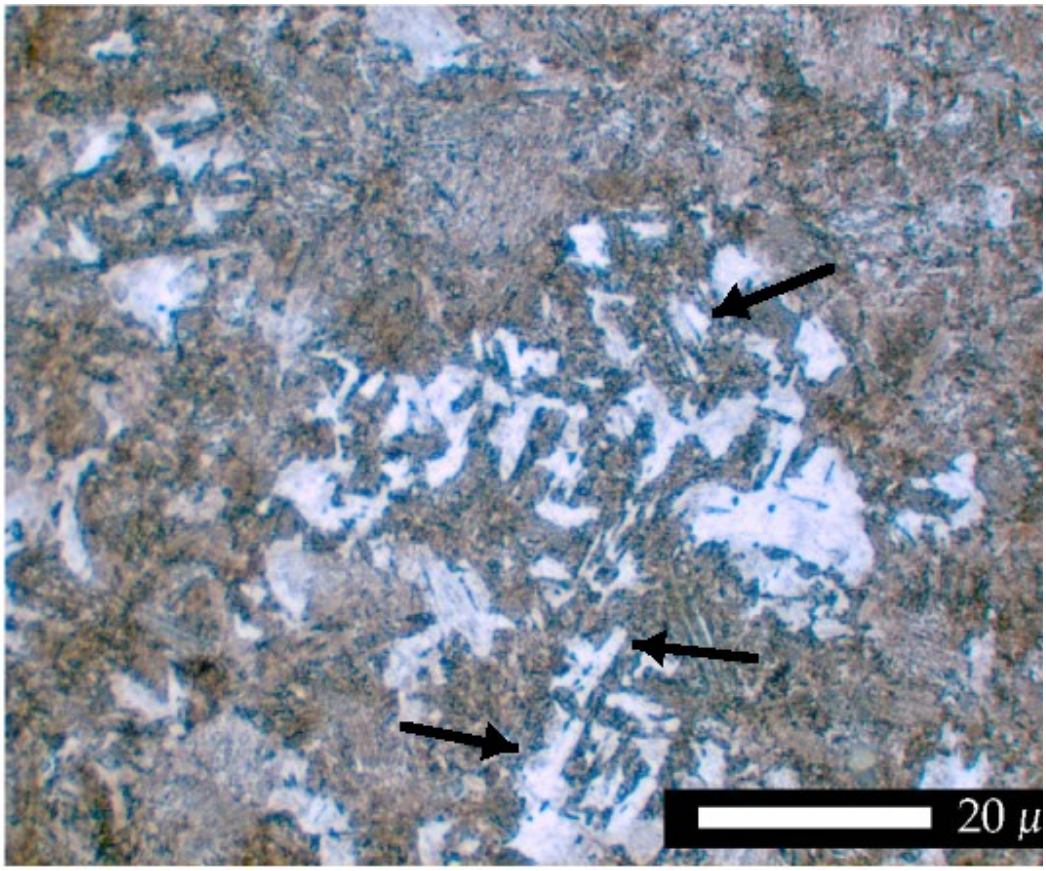

Figure 45: Notice the straight edges (arrowed) to the light-etching areas of martensite. These are also characteristic of a mixed microstructure of bainite and martensite, because bainite forms on specific crystallographic planes of austenite. The edges would not be so straight if the brown-etching phase was pearlite.

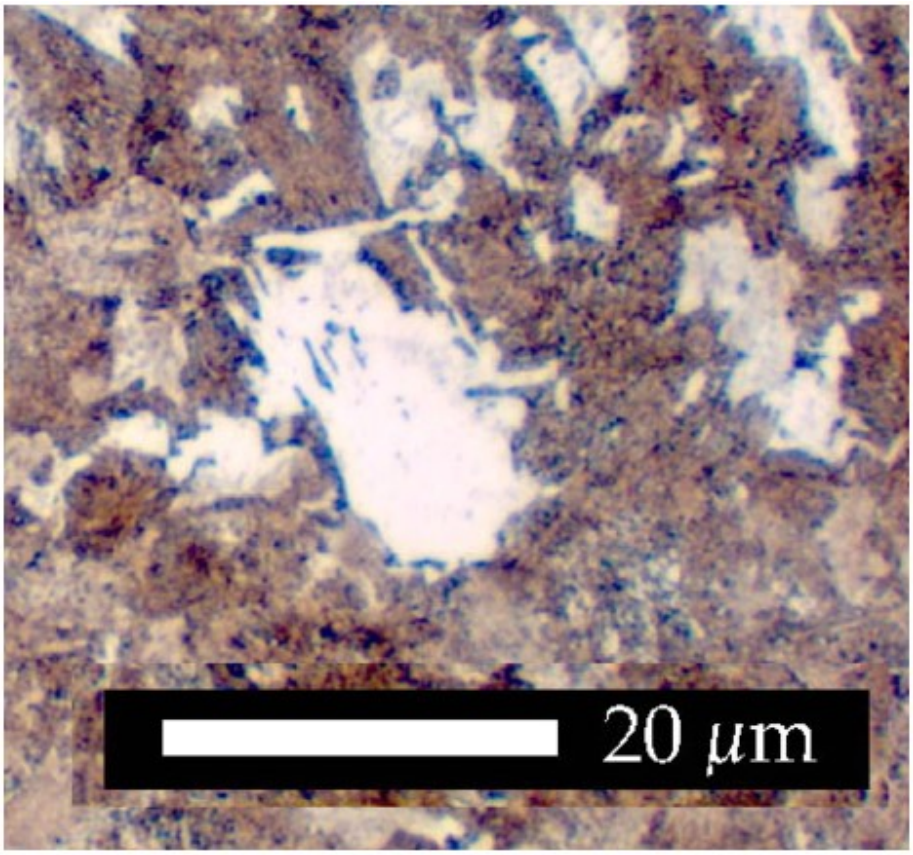

Figure 46: A higher magnification optical micrograph of a mixture of bainite and martensite. The straight edges are clear, and it is even possible to see the occasional bainite plate inside the light-etching phase which was originally austenite but is now untempered martensite.

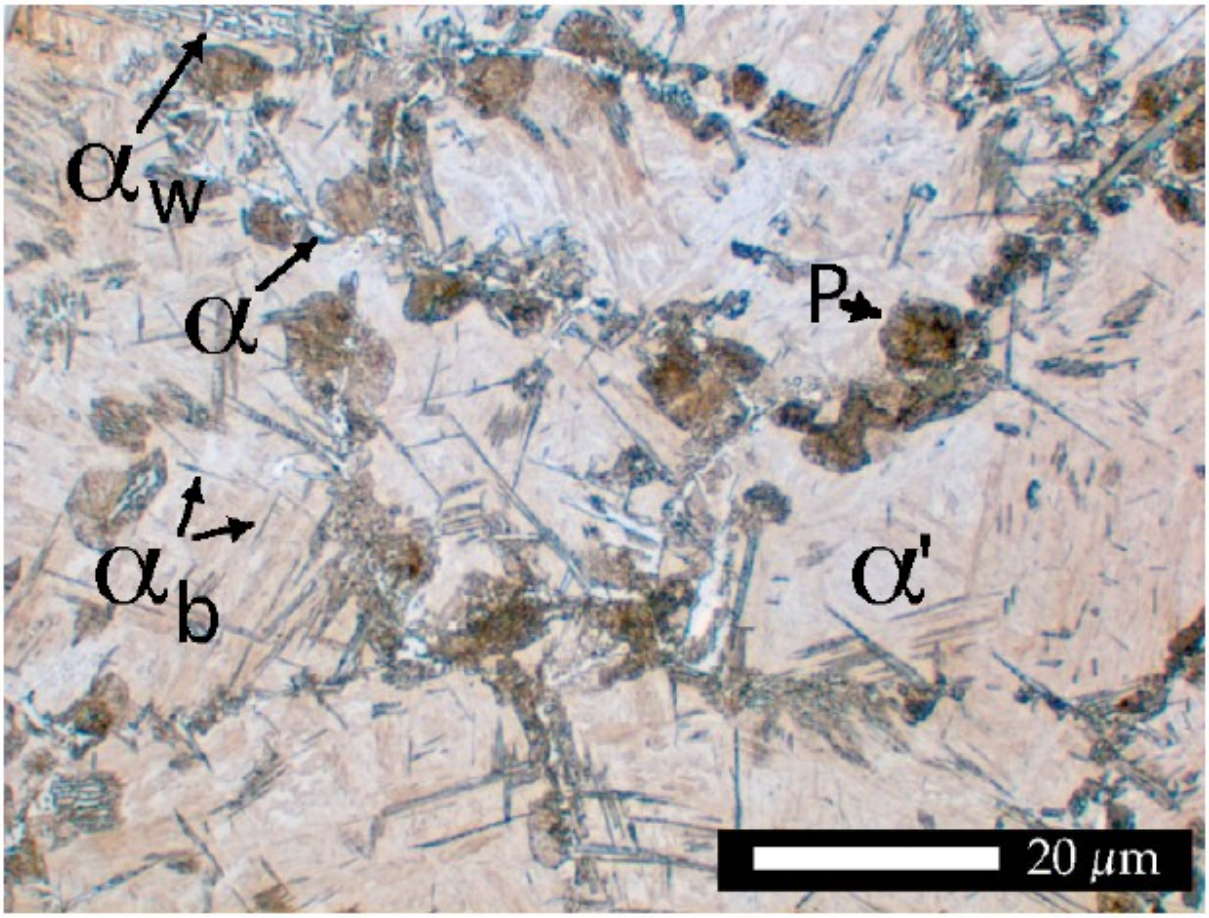

Figure 47: This is taken from the heat-affected zone of a weld in the coarse-austenite grain region. The microstructure is predominantly martensite but also has allotriomorphic ferrite, Widmanstätten ferrite, bainite and pearlite. Notice that the spherical shape of a pearlite colony is obvious in this sample because of the lack of impingment. Notice also that pearlite, unlike bainite, grows across the austenite grain boundaries. The Widmanstä ferrite plates are white because of the lack of structure within the plates, whereas bainite etches relatively dark.

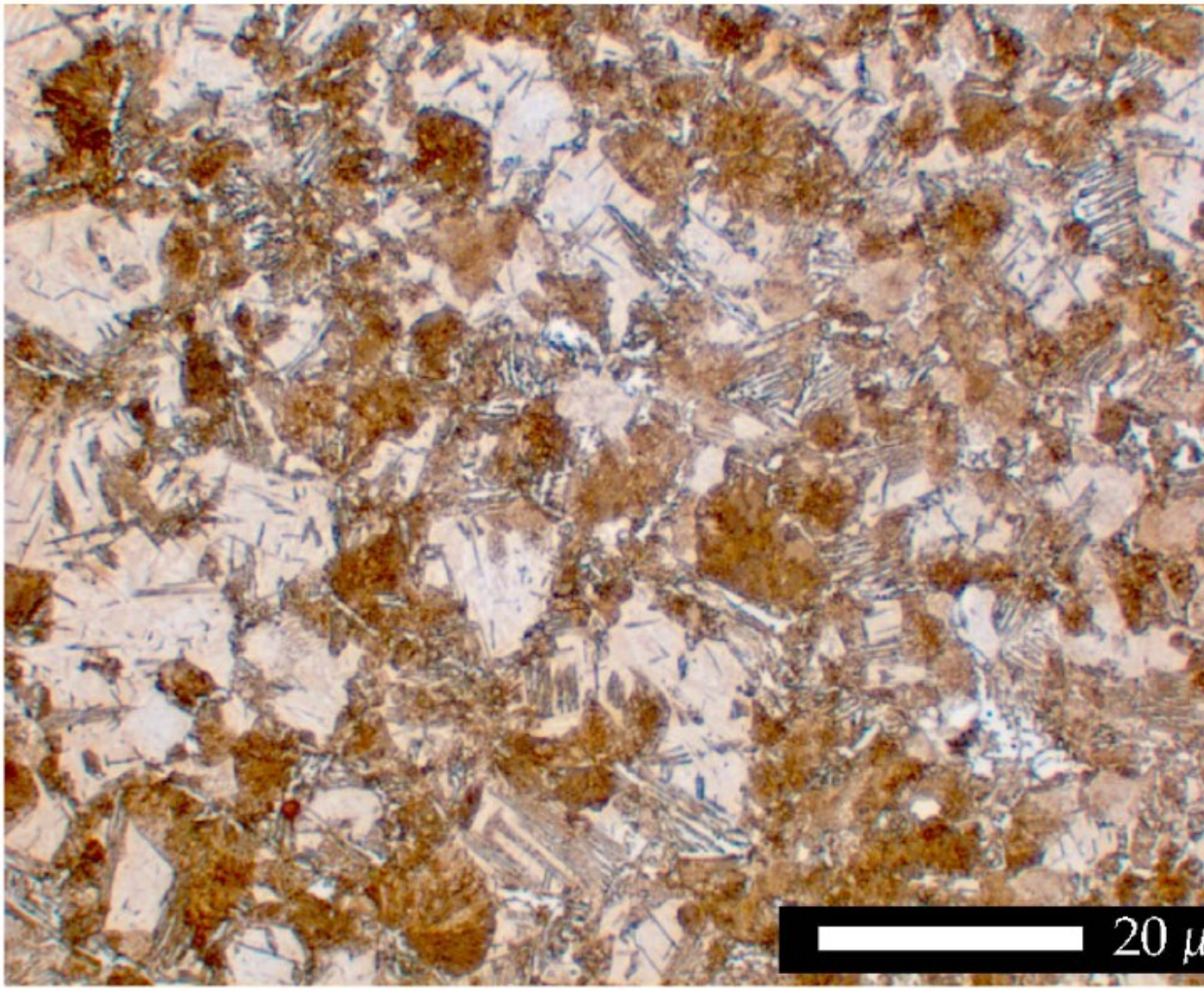

Figure 48: This is from a region further away from the fusion boundary, with smaller austenite grains and slower cooling rate. Thus, the amount of martensite is reduced. All the phases seen in Fig. 39 are evident here. The pearlite colonies are clear and seen to grow across the austenite grain boundaries. The optical microstructure would be more difficult to interpret in the absence of the untempered martensite. A combination of techniques would then be necessary to reveal its secrets.

Revealing the Prior Austenite Grain Structure

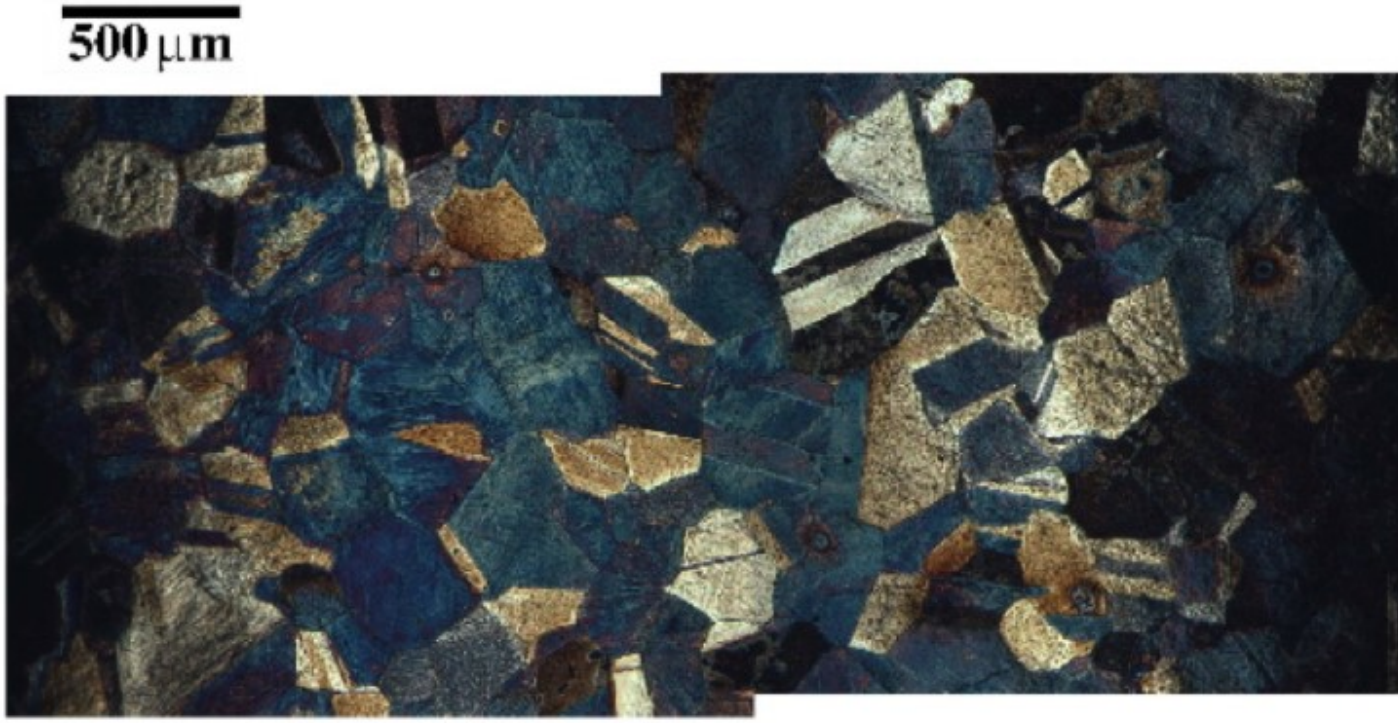

Figure 49: Thermal etching by partial oxidation of the polished sample surface at the austenitisation temperature. Micrograph courtesy of Mathew Peet.

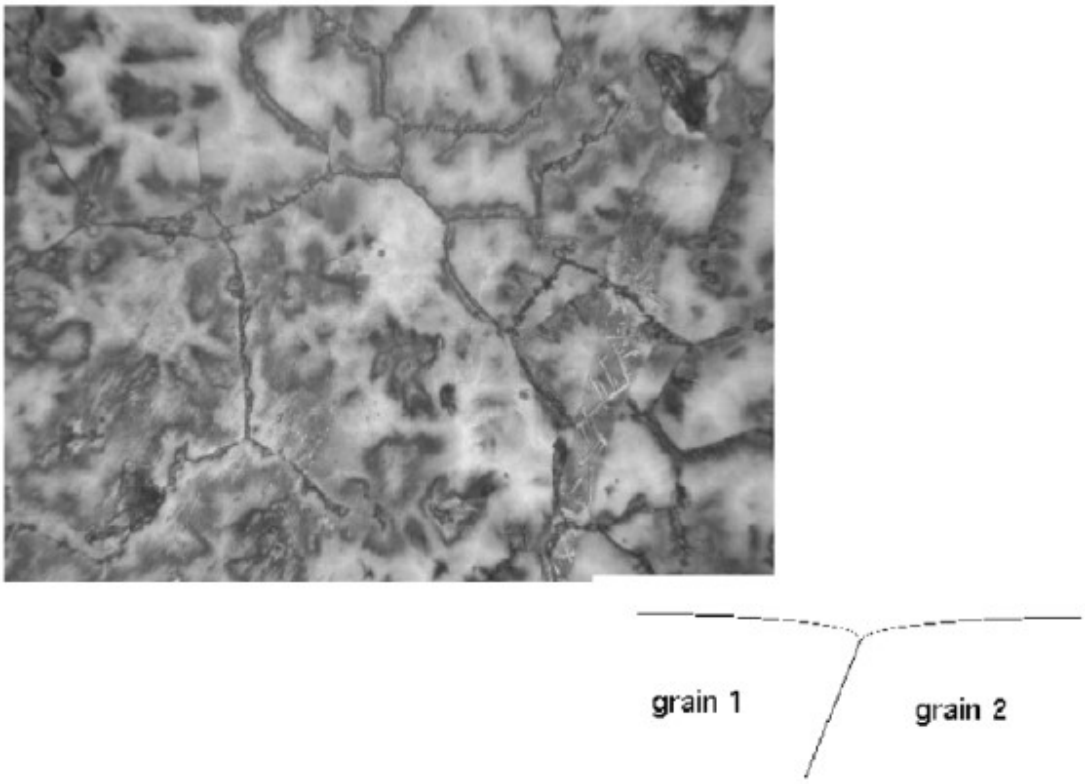

Figure 50: Polished sample held at austenitisation temperature. Grooves develop at the prior austenite grain boundaries due to the balancing of surface tensions at grain junctions with the free surface. Micrograph courtesy of Saurabh Chatterjee.